TU Delft

Delft University of Technology

Optimal Tuning of Fast P Support in Multi-area HVDC-HVAC Power Systems with Electrolyzers

Giannakopoulos, G.; Perilla, A.; Torres, J. L. Rueda

DOI
10.1109/ACCESS.2025.3640956

Publication date
2025

Document Version
Final published version

Published in
IEEE Access

Citation (APA)
Giannakopoulos, G., Perilla, A., & Torres, J. L. R. (2025). Optimal Tuning of Fast P Support in Multi-area HVDC-HVAC Power Systems with Electrolyzers. *IEEE Access*, *13*, 208454 - 208472. https://doi.org/10.1109/ACCESS.2025.3640956

Important note
To cite this publication, please use the final published version (if applicable).
Please check the document version above.

Copyright
Other than for strictly personal use, it is not permitted to download, forward or distribute the text or part of it, without the consent of the author(s) and/or copyright holder(s), unless the work is under an open content license such as Creative Commons.

Takedown policy
Please contact us and provide details if you believe this document breaches copyrights.
We will remove access to the work immediately and investigate your claim.

This work is downloaded from Delft University of Technology.
For technical reasons the number of authors shown on this cover page is limited to a maximum of 10.

IEEE Access
Multidisciplinary | Rapid Review | Open Access Journal

Received 22 October 2025, accepted 20 November 2025, date of publication 5 December 2025,
date of current version 12 December 2025.

Digital Object Identifier 10.1109/ACCESS.2025.3640956

APPLIED RESEARCH

Optimal Tuning of Fast P Support in Multi-Area HVDC-HVAC Power Systems With Electrolyzers

GEORGIOS GIANNAKOPOULOS, ARCADIO PERILLA, AND JOSÉ LUIS RUEDA TORRES, (Senior Member, IEEE)
Department of Electrical Sustainable Energy, Delft University of Technology (TUD), 2628 CD Delft, The Netherlands
Corresponding author: José Luis Rueda Torres (j.l.ruedatorres@tudelft.nl)

ABSTRACT HVDC-HVAC power systems dominated by power electronic converter interfaced elements are exposed to frequency instability risk due to low levels of system inertia and ineffective primary frequency control. Hence, significant research is devoted to new control concepts to enable fast active power (P) - frequency support by power electronic converters. Furthermore, when multiple elements attempt to arrest P imbalances, a coordinated strategy is required to avoid adverse consequences of concurrent and interfering control actions such as steep rate-of-change-of-frequency and over/under frequencies during the frequency containment period. To tackle this issue, in this paper, three different optimization strategies are formulated aiming at a cooperative reaction of fast P controllers attached to the outer control layer of modular multilevel converters (MMCs) applied in HVDC links and proton exchange membrane (PEM) electrolyzers. Each formulation is implemented by combining DIgSILENT PowerFactory 2024 SP2 as a power system simulation tool with a Python-based optimization solver that adopts the mean variance mapping optimization algorithm (MVMO). A comparative analysis performed on a multi-area multi-energy hybrid HVAC-HVDC power system to evaluate the proposed formulations in terms of their applicability, effectiveness according to P reserve availability, optimization convergence rate, and the suitability of the frequency response due critical sudden P imbalances.

INDEX TERMS Active power gradient, fast active power-frequency support, frequency controllers' tunning, mean-variance mapping optimization, MMC-HVDC links, PEM electrolyzers.

I. INTRODUCTION

New architectures of HVDC-HVAC power systems are emerging due to the energy transition [1], [2]. This entails the proliferation of power electronic converter interfaced elements in generation, demand, storage, compensation, and interconnectors of transmission and distribution systems [3]. Hence, the new systems exhibit unprecedented forms of dynamic behavior when disturbances occur [4]. For instance, frequency instability due to nonlinear frequency excursions, superimposed with poorly damped oscillations, constitutes a symptom of reduced resources and ineffective control for mitigating active power imbalances [5], [6]. In view of this challenge, significant research effort is currently devoted to new control concepts to enable fast frequency support (FFS) capability in power electronic converters [7]. Voltage source converters (VSCs) have positioned as the preferred converter technology, one reason being its high controllability [8], [9], [10]. Widespread applications of VSCs include renewable power plants [11], HVDC interconnectors [12], [13], storage devices [14], and responsive demand such as proton exchange membrane (PEM) electrolyzers [15]. Remarkably, VSCs are an attractive option for FFS, since they can quickly adjust their active power setpoints in response to frequency deviations [16]. Modern VSCs can inject/absorb active power at rates of even 1000 MW/s [8]. Active power gradient (APG) based control is among the preferred FFS concept. The APG attached to a VSC unit is usually designed according to local control targets [17]. Hence, research on coordinated design is needed to ensure effective collective deployment of the available active power headroom (ΔP) and the rate of active power adjustment (dP/dt) of VSCs [18], [19]. This paper

The associate editor coordinating the review of this manuscript and approving it for publication was Ragab A. El-Sehiemy.

© 2025 The Authors. This work is licensed under a Creative Commons Attribution 4.0 License.
For more information, see https://creativecommons.org/licenses/by/4.0/

sheds light on the way the optimal tuning of APG can be achieved leading to a coordinated FFS from different controllable active power sources belonging to a multi-area and multi-energy HVDC-HVAC system. Three different problem formulations are proposed to investigate the degree of effectiveness of optimal collective response of APG attached to modular multilevel converters (MMC) type of VSC applied in the system's HVDC links and PEM electrolyzers. The investigation on a multi-area system also goes beyond the current state-of-the-art by performing a systematic optimization oriented solution search instead of a basic parametric sensitivity analysis of APG that was previously performed by the authors on a two-area system with a point-to-point HVDC interconnection [20], [21], [22]. Each formulation is implemented by combining DIgSILENT PowerFactory 2024 SP2 as a power system simulation tool with a Python-based optimization solver that adopts the mean variance mapping optimization algorithm (MVMO) to find solution within a few optimization problem evaluations [23]. The paper continues with the following structure: Section II presents the multi-area test system. In Section III, problem formulations are discussed in detail. Section IV describes the application of the MVMO algorithm based solution of the formulations. Numerical analysis is presented in Section V, whereas the concluding reflections and outline of prospective follow-up research are condensed in Section VI.

II. THE TEST SYSTEM

In this research, the APG control strategy has been applied in a modified version of the PST16 benchmark system, which was originally presented in [24]. This benchmark is a three-area benchmark system with 16 synchronous generation units (SGUs) spread across the areas. The model is parametrized inspired from European systems and it is suited for stability studied based on RMS time-domain simulations [25]. The modifications comprise of the replacement of the three weak HVAC lines used to interconnect the three areas by MMC-based HVDC links and the replacement of 30% of the local demand of each area by large-scale PEM electrolyzers. These adjustments are in line with the expected hydrogen-based demand scenarios by 2050 as described in [26]. The electrolyzers have been installed at eleven different locations of the system to examine the distance dependent impact. For instance, some locations are close to synchronous generation units (SGUs), whereas others are close to the common coupling points (CCPs) with the HVDC links, or some electrolyzers are located at remote connection points.

For the representation of the MMC-based HVDC links, a dynamic model of DIgSILENT PowerFactory 2024 SP2, described in [27] and [28] has been chosen. The MMC-based HVDC link has 2 MMC stations interconnected by a bipolar configuration. The model details and reference parameters can be found in [29]. The converter at the sending end of the link operates as a rectifier, whereas the converter at the receiving end as an inverter. Their power output during steady state is provided based on the corresponding power flows among the areas on the original system [30]. The rectifier operates according to DC voltage (V_{dc_ref}) and reactive power setpoints (Q_{ref}) and the inverter according to active (P_{ac_ref}) and reactive power (Q_{ref}) setpoints to control the power injected in each area and to maintain the DC voltage of each HVDC link. The output of each station is controlled through a current vector control strategy as described in [31]. The representation of the PEM electrolyzers is based on a dynamic load model, equipped with a proportional fast P control as defined in [32]. The interconnection layout of the PEM electrolyzer is shown in Fig. 1 and its control structure is depicted in Fig. 2. The control adjusts the ramp rate of the P consumption of the electrolyzer within the feasible headroom [32].

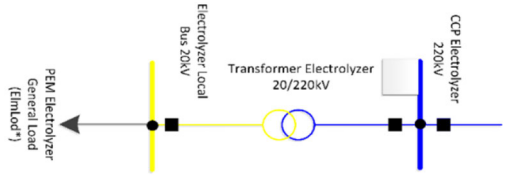

FIGURE 1. PEM electrolyzer's model in DIgSILENT PowerFactory.

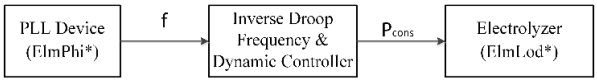

FIGURE 2. PEM electrolyzer's FFS layout in DIgSILENT PowerFactory.

A complete schematic diagram of the modified (i.e. HVDC-HVAC) PST16 benchmark system is shown in Fig. 3. The generated and demanded active power per synchronous area is summarized in Table 1. To perform FFS between the synchronous areas, the active power controller of the outer control loop of the inverter of each HVDC link is modified as proposed in Fig. 4. Note that the APG control block has been inserted into the loop to affect the active power output of the converter by considering the time evolution of the frequency responses of the interconnected synchronous areas participating in FFS. This change allows modulating the active power setpoint (P_{ac_ref}) of the HVDC link by ΔP following the occurrence of an active power imbalance. Based on the observed frequency response in several time-domain simulations of different disturbances (e.g. splitting between areas, sudden generation outages, or sudden demand increase/decrease), different system loading levels (low-medium-high demand) and parametric sensitivity assessment with different values of time delay (e.g. 0.001 s – 0.5s) it was empirically found that an activation time delay of 0.3s is (ideally) suitable for effective APG control in different situations. This assumption is in line with the delay ranges reported in fields tests done in [32] and [44]. Such assumed value for this study would be higher when considering communication latencies and converter response constraints. Nevertheless, the findings shown in Section V

of this paper still hold if it increases up to 0.5s. Reducing the total latency is a key research challenge that will be comprehensively addressed in a future follow-up publication. Performance metrics like Rate-of-Change-of-Frequency (e.g. which must be lower than 400 mHz/s) and Maximum Frequency Deviation (e.g. which must be lower than 200 mHz), which are described in [16] and [17], were computed in each time-domain simulation, and it was found that the aforesaid allowed thresholds were respected.

TABLE 1. Active power generation and demand per synchronous area.

	Generation (MW)	Demand (MW)
Area A	3150	1770
Area B	4000	4670
Area C	3130	3705
Total	10280	10145

Furthermore, another control block is also considerer to affect the rate-of-change in the active power setpoint. As shown in Fig. 4, this block is implemented in PowerFactory by using a rate limiter. The calibration of the parameters (ΔP and APG) of the added control blocks can be done by parametric sensitivity, like in the tuning method suggested in [16]. However, such method does not entail an optimally coordinated FFS support by all available resources. Hence, in this study, it is proposed to tackle it as an optimization problem. As elaborated in the subsequent section, the formulation and solution of such problem can be defined in different ways, respecting the technical limitations and the ramp-rate capabilities of the considered components involved in FFS. The FFS-modulated active power consumption by PEM electrolyzers is done by a supplementary inverse droop control block in combination with a rate limiter as proposed in Fig. 5.

Alternative supplementary control structures for FFS by PEM electrolyzers can be found in [32]. The implementation of these controller and a comparative assessment will be addressed in a future publication. Reference parameters for FFS by multi-megawatt PEM electrolysers are assumed [33], which considers an activation deadband of approximately 10mHz, also taking into account $\Delta f_{max} = 200$mHz. As shown in the subsequent section, each electrolyzer is optimally tuned regarding its bid size and ramp-rate. The proposed and compared optimization problem formulations consider predefined technical boundaries for the tuning of each of the parameters according to min-max bounds suggested in [22], [32], and [34].

III. COORDINATED TUNING OF APG CONTROL FOR FFS

The aim of this study is to examine the effectiveness of the APG control that can be collectively done by available resources. From an optimization perspective, such coordinated tuning can be formulated in different ways, e.g. different statement of the objective function (OF). This section proposes three different problem formulations and sheds light on the pros and cons by using a representative event that significantly challenges FFS due to a severe active power imbalance.

A. PROBLEM FORMULATION 1

In a multi-area power system, comprising k areas electromagnetically decoupled via MMC-based HVDC links, each area of the system is in principle characterized by a different frequency response. When an active power imbalance occurs in one of the areas, the balance between generation and demand in this area is perturbed, and its frequency tends to deviate from its nominal value. The frequency in the other areas remains intact if the HVDC links are not controlled to respond to this phenomenon. However, the controllers of the converter stations can be modified to respond to frequency deviations encountered in one of the interconnected areas.

In this case, the HVDC links share the imbalance to other areas that perceive a portion of the original disturbance as an active power imbalance that occurs at the CCPs of their HVDC links. Hence, each of the areas experiences different frequency deviations depending on the magnitude of the perceived active power imbalance, the underlying pre-disturbance operating conditions of each area, the area's inertia, and the available primary frequency reserves [4], [35]. The latter imbalances are handled by the local SGUs and power electronic interfaced (PEI) devices that are activated to provide FFS. In that way, the imbalance is shared among the k interconnected areas by utilizing the frequency containment reserves installed in all of them, achieving not only a rapid arrest of the frequency excursion in the affected area, but also the minimum propagating impact on the supporting areas.

In view of the above, problem formulation 1 aims at the minimization of the frequency excursions in all the k electromagnetically decoupled areas participating in frequency regulation, following the occurrence of an active power imbalance. As illustrated in Fig. 6, problem formulation 1 can be graphically represented as the sum of the graphical areas defined by the dynamic frequency response of each electrical area and the straight line that corresponds to the nominal frequency (e.g., 50 Hz). The goal of this problem formulation is to minimize the sum of the defined areas while attempting to obtain frequency responses that are closer to the nominal frequency.

Mathematically, problem formulation 1 is stated as follows:

Minimize:

$$OF1(\mathbf{x}) = \int_0^{\tau} w_A\,(f_A(\mathbf{x},t) - f_{nA})^2 + w_B\,(f_B(\mathbf{x},t) - f_{nB})^2 + \ldots + w_k\,(f_k(\mathbf{x},t) - f_{nk})^2 \quad (1)$$

subjected to:

$$\mathbf{x}_{min} \le \mathbf{x} \le \mathbf{x}_{max} \quad (2)$$

where $f_k(\mathbf{x},t)$ is the instantaneously measured frequency in the k-th area, f_{nk} is the nominal frequency of the k-th area,

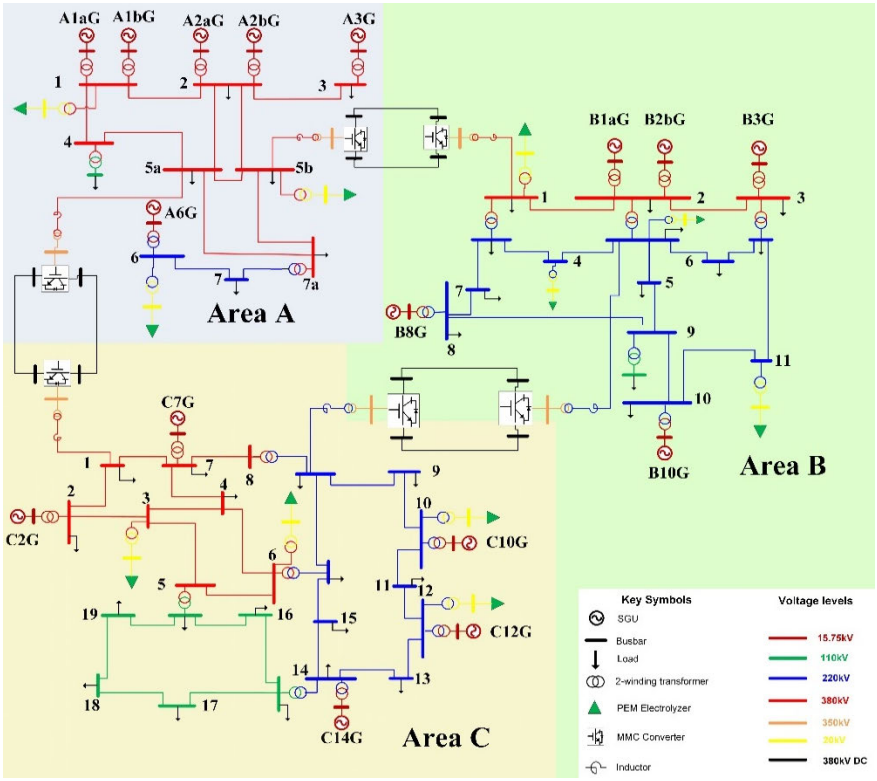

FIGURE 3. The modified PST 16 benchmark system.

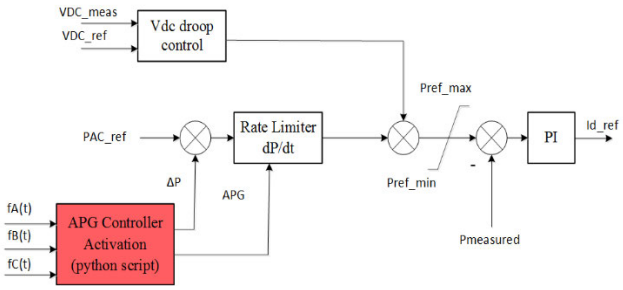

FIGURE 4. Modified P/V_{DC} controller of the MMC-HVDC for FFS.

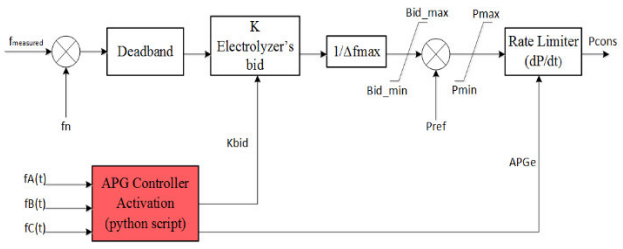

FIGURE 5. PEM electrolyzer's supplementary control for FFS.

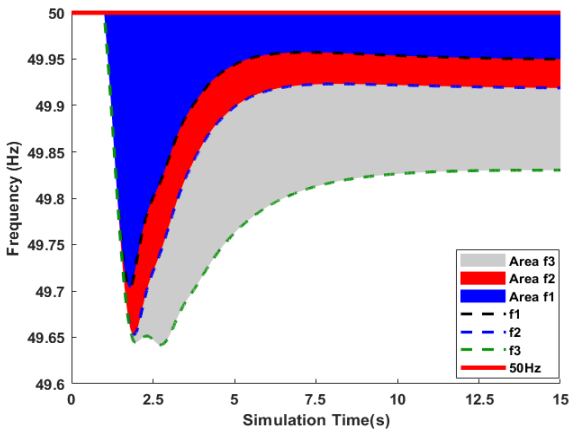

FIGURE 6. OF1 representation – Minimization of the graphical areas between the frequency response of each electrical area and the nominal frequency.

and w_k is a weighting factor. In this study, w_k is set to 1 to give equal priority to the frequency regulation in all areas. A more sophisticated approach is needed find the most suitable weighting factors while accounting for different aspects that influence the inherent diversity of dynamic frequency response of each interconnected synchronous area. For instance, an extended optimization problem formulation could be done to co-optimize the weighting factors. This topic is being tackled in ongoing research and will have a dedicated in-depth discussion in a subsequent publication.

The optimization vector **x** comprises of 2 optimization variables for each of the PEI devices that participate in FFS. For HVDC links, the first optimization variable represents the

new active power setpoint defined by the change (ΔP_{HVDCi}) in its power flow, whereas the second one represents the ramp rate at which the change of the active power is applied on the AC side of the inverter station (APG_{HVDCi}). For PEM electrolyzers, the first optimization variable represents the bid size of the electrolyzer (K_{ebidj}), which corresponds to the proportional gain of its frequency controller. The second optimization variable represents the ramp rate at which the changes in the power consumption of each unit are performed (APG_{ej}). Since the modified PST 16 benchmark system has 3 MMC-based HVDC links and 11 PEM electrolyzers, it is considered that 28 optimization variables form the optimization vector $\mathbf{x}$ at its full extend, which implies that all elements participate in FFS. Generally speaking, in case of α HVDC links and β PEM electrolyzers available for FFS in any multi-area system, the optimization vector $\mathbf{x}$ contains $2\alpha+2\beta$ optimization variables as illustrated in (3), as shown at the bottom of the next page.

Each of the considered optimization variables is bounded within its acceptable limits. These are derived mainly from the technical limitations of each unit. For the HVDC links, the active power flow should not overcome the rated capacity of the link in both directions as defined in (4) [20], [21], [22]. Also, as explained in [36], the maximum ramp rate that the MMC station can handle cannot overcome a certain rate, as denoted in (5).

$$P_{\text{refi}} + \Delta P_i \leq \left|P_{\text{rated}\,i}\right| \tag{4}$$

$$0\frac{\text{GW}}{\text{min}} \leq \text{APGi} \leq 60\frac{\text{GW}}{\text{min}} \tag{5}$$

For the PEM electrolyzers, the available bid size may vary from 0 to 70% of their rated capacity according to the availability of each unit, as a 30% of its rated capacity is considered as a minimum limit of its power consumption [32]. Furthermore, the ramp rate of the consumption of these units should be bounded by the maximum rate they can handle. In this paper, a fast active power ramp rate of 0.5 pu/s is assumed. This value is in line with reference active power ramp rates of the latest technologies, which are indicated in [32], [34], and [37], e.g. PEM technologies have active power ramp rates in the range 10 %/s – 50 %/s. Furthermore, the assumed bounds have been validated by real-time digital simulations (including hardware-in-the-loop tests) and field measurements done in an actual electrolysis plant located in the north of the Netherlands [32], [34]. The boundary conditions applied for the PEM electrolyzers are summarized in (6) and (7).

$$0 \leq \text{K}_{\text{bid}_\text{w}} \leq 0.7\text{P}_{\text{elec rate w}} \tag{6}$$

$$0 \leq \text{APG}_{\text{e}_\text{w}} \leq 0.5\text{P}_{\text{elec rated w}}\,\frac{\text{MW}}{\text{s}} \tag{7}$$

B. PROBLEM FORMULATION 2

In this proposed problem formulation, the frequency stability of the system is evaluated with respect to the trajectories of the dynamic displacements of the areas' relative speeds. In a single area system, the relative speed of the system during pre-disturbance steady state conditions can be represented as a vector of a constant length equal to 1. When the active power balance of the system is perturbed, the length of the vector (representing the area's speed and thus its relative frequency) changes at a rate determined by the rate-of-change-of-frequency (RoCoF). The length of the vector becomes larger than 1 in case of an over-frequency event, and smaller than 1 in case of an under-frequency event. Thus, to arrest any frequency deviation, the magnitude of the changes determined in the vector length due to occurrence of an active power imbalance must be minimized. This can be done by minimizing the rate of change of the dynamic displacement of the area's relative speed.

In case of a multi-area system decoupled by MMC-based HVDC links, in which each area is characterized by its own frequency dynamics, multiple vectors can be used to represent the total systems' frequency behavior both separately (from a local area perspective) and combined (from a system wide perspective). For sake of illustration, considering the 3-area electromagnetically decoupled system of interest in this study, 3 vectors evolving in 3 different directions x, y and z can be used to represent the system's frequency, forming a frequency cube shown in Fig. 7. When an active power imbalance occurs, the volume and the geometrical shape of the frequency cube change according to the resulting frequency deviation and the RoCoF in each area.

According to this representation, the goal of problem formulation 2 is to minimize any volumetric changes in the frequency cube and coordinately manage FFS based on the rate of change of the volumetric changes in each direction with respect to the steady state representation of the frequency cube, as shown in Fig. 7 in light blue. This entails that problem formulation 2 optimally allocates the share of FFS among all participating PEI devices, leading to an optimal sharing of the imbalance among the electrical areas according to their primary frequency control characteristics (which are defined by their inertial heterogeneity and P-f response disparities). In that way, it is expected that the dynamic frequency excursions are mitigated as quickly as possible, implying an attempt to steer relatively (i.e. reaction bounded by each area's physical properties) similar frequency responses in the different electrical areas due to the coordinative support from the HVDC links and the support from the installed PEM electrolyzers.

For the mathematical representation of this problem formulation, the relative speed of each area should be calculated based on the synchronously rotating masses of each area. If the n SGUs of the k-th area have similar inertia and power rating characteristics, the area's speed (ω_k) can be calculated based on the average speeds of the actively operating SGUs at every instant as shown in (8) [20]. Alternatively, to take into account the inertia constants of the operating SGUs, the relative speed of the k-th area can be calculated according to the center of inertia (COI) of each area as shown in (9) and explained in [38]. It is assumed that the wide-area monitoring

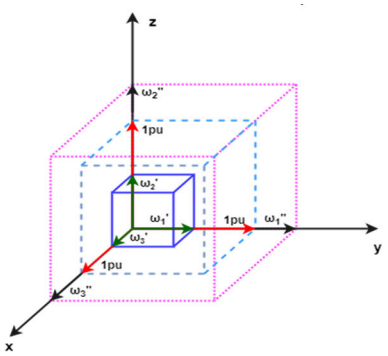

FIGURE 7. Illustration of the objective function of problem formulation 2 for a three-area system – Minimization of volumetric changes of the frequency cube compared to the nominal 1 p.u. cube.

system has enough measured data (e.g. PMU) to calculate or synthesize the speeds. Hence, according to the calculation method used, 2 different versions of OF2, the average-based OF2 and the COI-based OF2 can be defined.

$$\omega_{\mathrm{k}}(\mathrm{t}) = \frac{\sum_{\mathrm{i}=1}^{\mathrm{n}} \omega_{\mathrm{ik}}(\mathrm{t})}{\mathrm{n}} \tag{8}$$

$$\omega_{\mathrm{kCOI}}(\mathrm{t}) = \frac{\sum_{\mathrm{i}=1}^{\mathrm{n}} \mathrm{H_i}\, \mathrm{S_{Bi}} \omega_{\mathrm{ik}}(\mathrm{t})}{\sum_{\mathrm{i}=1}^{\mathrm{n}} \mathrm{H_i}\, \mathrm{S_{Bi}}} \tag{9}$$

where $\omega_{\mathrm{ik}}(\mathrm{t})$ is the instantaneous speed of the i-th SGU in the k-th area at the t time instant, n is the number of the actively operating SGUs in the k-th area, $\mathrm{H_i}$ is the inertia constant of the i-th SGU in s and $\mathrm{S_{Bi}}$ is the rated power of the i-th SGU in MVA.

Having calculated the speed of each area throughout the whole simulation period, the frequency cube can be expressed volumetrically at every time instant by using (10).

$$v(t) = \prod_{j=A}^{k} \omega_j(t) \tag{10}$$

Then, objective function of problem formulation 2 (OF2) can be mathematically expressed for the 3-area system of interest by using equations (11) to (13).

Minimize:

$$\mathrm{OF2}(\mathbf{x}) = \frac{\mathrm{d\,V}(\mathbf{x}, \mathrm{t})}{\mathrm{dt}} = \frac{d\omega_{\mathrm{A}}(\mathbf{x}, \mathrm{t})}{\mathrm{dt}} \omega_{\mathrm{B}}(\mathbf{x}, \mathrm{t}) \omega_{\mathrm{C}}(\mathbf{x}, \mathrm{t}) + \frac{\mathrm{d}\omega_{\mathrm{B}}(\mathbf{x}, \mathrm{t})}{\mathrm{dt}} \omega_{\mathrm{A}}(\mathbf{x}, \mathrm{t}) \omega_{\mathrm{C}}(\mathbf{x}, \mathrm{t}) + \frac{\mathrm{d}\omega_{\mathrm{C}}(\mathbf{x}, \mathrm{t})}{\mathrm{dt}} \omega_{\mathrm{A}}(\mathbf{x}, \mathrm{t}) \omega_{\mathrm{B}}(\mathbf{x}, \mathrm{t}) \tag{11}$$

subjected to

$$\frac{\mathrm{d}\omega_{\mathrm{A}}(\mathbf{x}, \mathrm{t})}{\mathrm{dt}} = \frac{\mathrm{d}\omega_{\mathrm{B}}(\mathbf{x}, \mathrm{t})}{\mathrm{dt}} = \frac{\mathrm{d}\omega_{\mathrm{C}}(\mathbf{x}, \mathrm{t})}{\mathrm{dt}} \tag{12}$$

$$\mathbf{X}_{\min} \leq \mathbf{X} \leq \mathbf{X}_{\max} \tag{13}$$

Like in problem formulation 1, the optimization vector $\mathbf{x}$ comprises of 2 optimization variables for each of the contributing FFS devices. The first one affects the amount of active power change in the active power setpoint of either the power flow in the HVDC link or the consumption of the electrolyzer and the second one the ramp rate of the change in the active power output performed in each device. The complete optimization vector $\mathbf{x}$ is as given in (3). Besides, the bounds for the optimization variables are defined in (4)-(7).

C. PROBLEM FORMULATION 3

In this problem formulation, for the representation of the frequency stability problem in the 3-area system considered in this study, three different frequency responses, i.e., one for each of the electromagnetically decoupled areas, are used. The frequency of each area can be measured at any bus of the area embodying the active power balance between generation and demand in the corresponding area. In case multiple areas actively participating in the frequency regulation, the goal of the tuning is to share the imbalance among the areas according to their inertia characteristics, the frequency control characteristics of their SGUs and the available active power reserves for FFS. Based on this representation, problem formulation 3 attempts to achieve an artificially coupled frequency response for an electromagnetically decoupled system. This can be done by minimizing the graphical area defined by each pair of the dynamic frequency responses of the electrical areas participating in frequency regulation after the occurrence of the imbalance, as illustrated in Fig. 8. This implies that this problem formulation attempts to achieve a similar dynamic shape of the frequency responses of the areas, which is expected to lead also to responses as close as possible to the nominal frequency. In contrast to problem formulation 1, which tries to minimize the area of each response from its nominal value as shown in Fig. 6, problem formulation 3 aims at minimizing the area among each pair of responses, thus, optimally sharing the imbalance among the electrical areas (cf. Fig.8).

Mathematically, problem formulation 3 has the format shown in (14) and (15).

Minimize:

$$\mathrm{OF\,3}(\mathbf{x}) = \int_0^{\tau} [|\mathrm{f_A}(\mathbf{x}, \mathrm{t}) - \mathrm{f_B}(\mathbf{x}, \mathrm{t})| + |\mathrm{f_B}(\mathbf{x}, \mathrm{t}) - \mathrm{f_C}(\mathbf{x}, \mathrm{t})| + |\mathrm{f_A}(\mathbf{x}, \mathrm{t}) - \mathrm{f_C}(\mathbf{x}, \mathrm{t})|\, \mathrm{dt}] \tag{14}$$

subjected to:

$$\mathbf{X}_{\min} \leq \mathbf{X} \leq \mathbf{X}_{\max} \tag{15}$$

The optimization vector $\mathbf{x}$ is defined and bounded as in the previous 2 problem formulations represented by equations (3)-(7).

$$\mathbf{x} = \begin{bmatrix} \Delta \mathrm{P_{HVDC_1}}, \mathrm{APG_{HVDC_1}}, \ldots, \Delta \mathrm{P_{HVDC_i}}, \mathrm{APG_{HVDC_i}}, \mathrm{K_{ebid_1}}, \\ \mathrm{APG_{e_1}}, \ldots, \mathrm{K_{ebid_j}}, \mathrm{APG_{e_j}} \end{bmatrix} \tag{3}$$

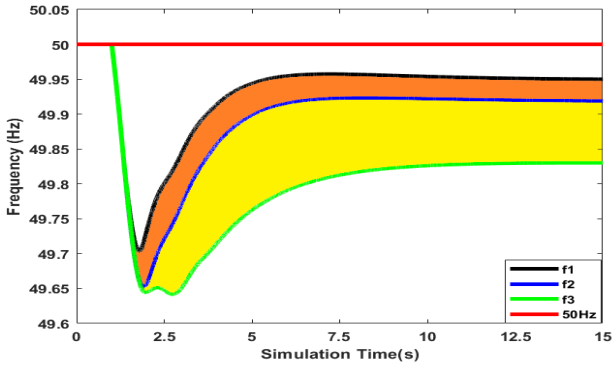

FIGURE 8. Representation of the objective function of problem formulation 3 – Minimization of graphical areas between each pair of frequency responses.

IV. OPTIMIZATION PROCESS

In order to solve the optimization problem and tune the fast active power - frequency controllers in each of the 3 proposed problem formulations, a co-simulation environment between Python 3.8 and DIgSILENT PowerFactory 2024 SP2 is developed.

DIgSILENT PowerFactory 2024SP2 is used to model the system comprising all its different components along with their control structures and to perform the required RMS simulations to obtain the dynamic response of the system. Python 3.8 has been utilized for the development of python scripts for each of the proposed problem formulations. Also, a python script is used to control DIgSILENT PowerFactory 2024 SP2 in order to apply the required changes in the parameters of the APG controllers of the FFS devices according to the evolving optimization vector. Additionally, the latter script controls the execution of the RMS simulations performed in DIgSILENT PowerFactory 2024 SP2, whose results are required for the calculations within each of the optimization problems. Finally, for the solution of the optimization problem a python-based version of MVMO algorithm has been developed based on [23]. This algorithm has been selected due to the fast convergence rate and the quality of results that it has achieved in other complex optimization problems of electrical power systems, cf. References [20], [21], [22], [23]. A schematic of the application of MVMO is shown in Fig. 9.

The MVMO algorithm generates an evolving (i.e., offspring) solution by performing a series of iterations based on the best achieved parent solution throughout the search and the statistical data representing the direction of the evolution of the optimum solution used by a mapping function for each of the evolved optimization variables. It performs the first iteration based on an initial optimization vector $\mathbf{x_0}$ either defined by the user based on operational experience or randomly calculated within the algorithm. Then, the candidate optimization variables are applied in the corresponding FFS devices modelled in DIgSILENT PowerFactory 2024 SP2, and a RMS simulation is executed to obtain the frequency response's time series of interest. The simulation results are

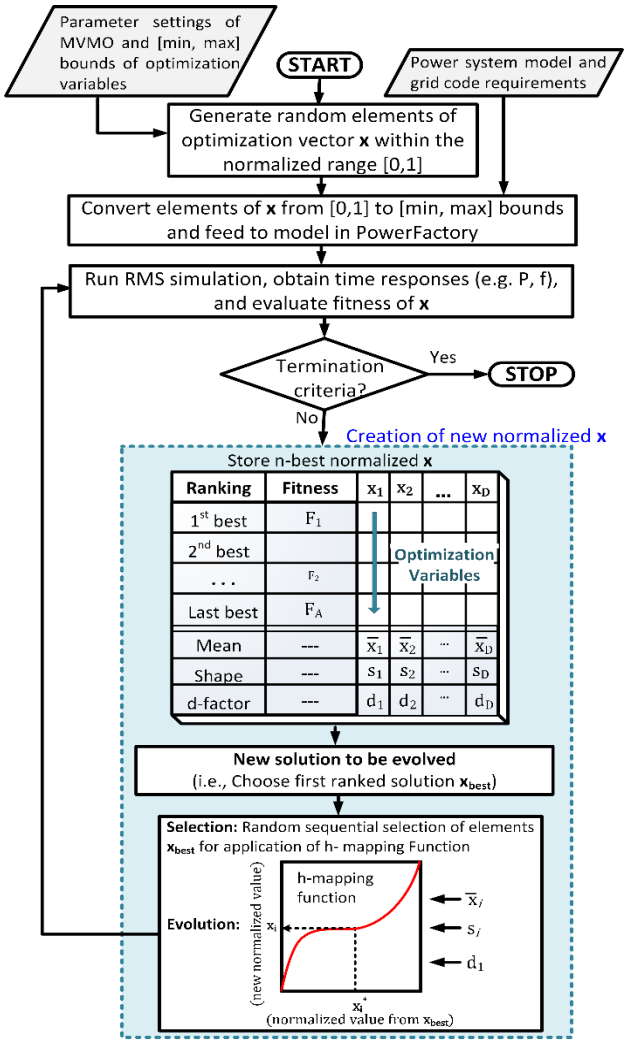

FIGURE 9. The mean variance mapping optimization (MVMO) algorithm.

stored in a csv file in a readable form by python and are used to perform the optimization problem evaluation. Then, several problem evaluations are performed having the solution vector evolving based on the candidate vectors that achieved the best fitness evaluations so far and the application of a mapping function until the termination criterion has been fulfilled. For this purpose, an archive of a constant size stores the best optimization vectors achieved so far along with statistical data for each of the optimization variables. Also, the algorithm generates the offspring solutions in a normalized [0,1] range respecting always in that way the boundaries of the optimization variables and avoiding penalties and modifications at a later stage [23]. In this study, a termination criterion corresponding to a number of 100 fitness evaluations has been selected based on a heuristic tuning of MVMO.

V. SIMULATIONS AND ANALYSIS OF RESULTS

To examine the differences between the proposed problem formulations and to define the one that achieves the

best tuning of the APG controllers, RMS simulations are performed, which illustrate the performance of the APG controllers when the worst underfrequency occurs in the modified PST 16 benchmark system. Such underfrequency is caused by the sudden loss of the largest generating unit (i.e., SGU A1a) in area A. Due to the low inertia conditions, the outage of the largest generating unit in area A leads to the most abrupt dynamic frequency excursion. The simulation event is applied on the system at t=1s and the RMS simulation is performed for a time window of 15s at a step of 0.01 to capture the dynamic frequency response of the system before and after the occurrence of the active power imbalance. Apart from the simulation event, for comparison purposes, in all the different scenarios shown in this section, the same pre-disturbance conditions have been considered. Also, in all illustrated scenarios, the optimization problem is characterized by the same initial settings for MVMO, which were taken from [23]. A performance comparison between MVMO and two selected alternative solvers from the current state-of-the-art is provided in the appendix.

According to the availability of the PEI considered to provide FFS and the examined optimization problem formulation, different scenarios have been defined. Hence, for sake of illustrative analysis, four sub-scenarios for the different proposed problem formulations (i.e., OF1, average-based OF2, COI-based OF2, OF3), which are summarized in Table 2, are investigated. In the first group of sub-scenarios, FFS is only provided by HVDC links trying to share the imbalance among the areas according to their generation and inertia characteristics. In the second group of sub-scenarios, FFS is not only provided by the HVDC links' modulated active power transfers but also by the PEM electrolyzers installed in the 3 areas. In that way, the effectiveness of each problem formulation can be examined both when the optimization vector $\mathbf{x}$ has a relatively small size (i.e., 6 optimization variables in the first group of sub-scenarios) and when $\mathbf{x}$ is at its full extend (i.e., 28 optimization variables in the second group of sub-scenarios).

TABLE 2. Investigated case studies.

Case studies	Available FFS assets	Tuning method	OF value
Scenario 1a	HVDC links	OF1	7.3434
Scenario 1b		OF2-average	0.5324
Scenario 1c		OF2-COI	0.5312
Scenario 1d		OF3	0.368
Scenario 2a	HVDC links + PEM electrolyzers	OF1	7.3434
Scenario 2b		OF2-average	0.5324
Scenario 2c		OF2-COI	0.5312
Scenario 2d		OF3	0.368

In order to evaluate the achieved performance when tuning the APG controllers by using any of the three different problem formulations, the obtained frequency responses are comparatively analyzed. For this purpose, a baseline scenario, which corresponds to the case when none of the PEI elements provides FFS, is taken as reference. Hence, the frequency containment is exclusively based on the fast active power - frequency control actions of the SGUs in the affected area, and then it is modified by the reaction of the added HVDC links and PEM electrolyzers. The frequency response of the system in the baseline scenario can be observed in Fig.10. In this case, the frequency in area A drops rapidly to 48.8Hz at a rate of −0.51Hz/s, and, due to the action of primary active power - frequency control in SGUs, it stabilizes at 49.55Hz, violating the post-disturbance operating state bounds, cf. example bounds defined in [39] and [40]. At the same time, the frequency in areas B and C remains constant at 50Hz, as these areas are electromagnetically isolated from area A due to the MMC-based HVDC links. Note that from the baseline scenario, optimally coordinated FFS from the PEI elements is more than necessary to maintain the frequency of the system within the acceptable normal operating limits. Finally, for comparison purposes, the value of each OF (i.e. OF1, average-based OF2, COI-based OF2 and OF3) has been calculated in the baseline scenario to highlight its improvement after the optimal and coordinated tuning of the controllers. The value of each OF in the baseline scenario can be observed in the last column of Table 2.

The effectiveness that can be achieved by using each problem formulation has been examined considering the conditions for applicability of each problem formulation, the number of problem (fitness) evaluations required considering a different size of the optimization vector, the convergence rate of the OF value, and the achieved frequency responses in the affected and the supporting areas following the considered critical active power imbalance. The latter one refers to the observed frequency Nadir, the RoCof, and the post-disturbance steady-state deviation in each area.

A. SCENARIO 1

In this case study, FFS is provided to the affected area A by modifying the power flows in HVDC links. This action is done by the APG controller attached to the inverter station of each HVDC link after its tuning based on one of the proposed problem formulations. The frequency responses obtained when the tuning of the APG controllers is performed under OF1, average-based OF2, COI-based OF2, and OF3 are observed in Figs. 11(a) to 11(d), respectively.

In all examined cases, during the first second of the simulation, the frequency in all areas is at the nominal value of 50Hz. At t=1s, the SGU A1a (the largest unit in area A) is lost, causing a fast frequency decrease in area A.

The frequency in areas B and C remains unaffected for 300 ms following the disturbance due to the activation time delay applied to the APG controllers of the HVDC links. After that time delay, the HVDC links change their power flows according to the solution of the optimization problem with respect to the minimization of the corresponding OF value (i.e. OF1, OF2 or OF3).

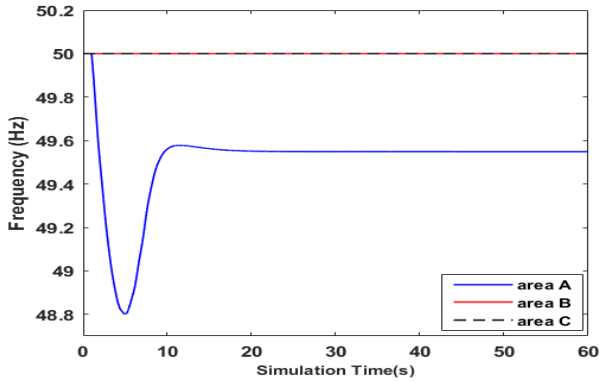

FIGURE 10. – Baseline Scenario - Areas' Frequency Responses due to the loss of SGU A1aG.

From the obtained frequency shown in Figs. 11(a) to 11(d), it can be observed that all OFs can be effectively used to tune the controllers against the active power imbalance, preserving the frequency in all areas within acceptable values of frequency Nadir and RoCof. This means, that compared to the baseline case, the activation of FFS can lead the system's frequency within the acceptable limits, cf. desired compliance within bounds given in [39] and [40]. Also, all problem formulations can effectively tune the APG controllers when the size of the optimization vector x is relatively small containing six optimization variables as explained in Section III.

Comparing the frequency responses following the tuning of the controllers, it is evident that OF1 (cf. Fig. 11(a)) achieves the best frequency response for the affected area, as it experiences a Nadir of 49.71Hz and subsequently it stabilizes around 50mHz away from the nominal frequency. The encountered RoCof in area A is equal to -0.38Hz/s being significantly improved compared to the baseline scenario (cf. Fig. 10). The other two areas contribute to the frequency containment after the activation of the APG controller of the HVDC links, and subsequently they stabilize around 49.85Hz, 150mHz away from 50Hz. In short, the use of OF1 implies that the frequency in the affected area can be effectively contained since HVDC links enable the share of the imbalance to the other areas with respect to their response to active power imbalances. However, recalling also that the weighting factors wk considered in OF1 are set to 1 in this study to give equal priority to the frequency regulation in all areas (cf. Section II.A, page 4), there is a risk that the frequency in supporting areas stabilizes with larger post disturbance steady state deviations compared to the affected area. The latter is evident in Fig. 11a as the frequency responses of the supporting areas converge at lower level compared to the frequency of area A. For sake of comparison, two alternative situations are considered here to further reflect on the implication of choosing the value of wk. In the first situation, wk=1 is assumed for area A, whereas wk=0.5 is assumed for areas B and C. In this case, a higher value of OF1 (i.e., OF1=7.9518) was obtained,

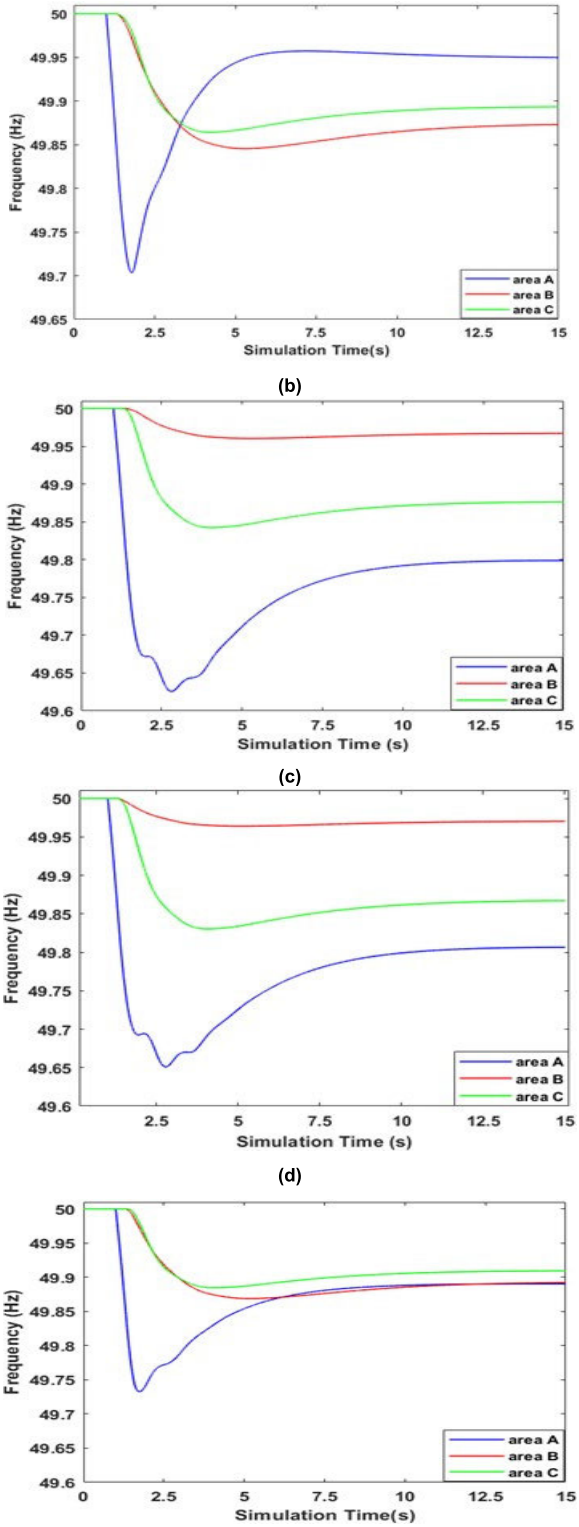

FIGURE 11. Frequency responses Scenario 1 – FFS by HVDC links: (a) tuning OF1; (b) tuning average-based OF2; (c) tuning COI-based OF2; (d) tuning OF3.

implying relatively lower improvements in Nadir and RoCoF for area A (Nadir=49.32Hz, RoCoF=−0.41Hz/s). Furthermore, the other two areas contributed less to the frequency

containment in the disturbed area A after the activation of the APG controller of the HVDC links, and they deviated less from the nominal frequency w.r.t. their performance in Fig. 11(a) and they stabilized around 49.89 Hz. This observed deterioration of OF1 is attributed to the fact that a higher value of wk for the affected area entails a stronger emphasis on the deployment FFS of this area, limiting the fast active power support from other areas (through the HVDC interconnectors) while reducing the collateral impact on the frequency performance of these supporting areas. The level of deterioration can be higher if the affected area has limited or lower FFS capabilities. In the second situation, wk=0.5 is assumed for area A, whereas wk=1 is assumed for areas B and C. In this case, a higher deterioration of OF1 (i.e., OF1=8.1937) was obtained, implying significantly lower improvements in Nadir and RoCoF for area A (Nadir=49.07Hz, RoCoF=-0.45Hz/s). This is due to the lower support from the other two areas to the frequency containment in the disturbed area, since their higher values of wk entail that the optimization prioritize the minimization of the collaterally caused frequency deviations in these areas (they stabilized around 49.95 Hz). This aspect must be specially taken into account if FFS support is required from areas with lower levels of inertia which could have higher vulnerability to collaterally caused active power imbalances. In line with the theoretical definitions in Section II.A, these findings highlight the need of a more sophisticated problem formulation to co-optimize the weighting factors. Finally, a simple sensitivity check was done w.r.t. the APG activation delay by considering two alternative values. For instance, Nadir≈49.87 Hz and RoCoF≈-0.27Hz/s were obtained when the delay is between 50-100ms, whereas Nadir≈49.52Hz and RoCoF≈-0.40Hz/s were obtained when the delay is between 400-500ms.

When OF3 (cf. Fig. 11(d)) is applied, the frequency nadir encountered in the affected area has a similar value with the one obtained when OF1 is used. However, it is shown that the RoCof in area A improves more than in case of OF1 (i.e. -0.34Hz/s with OF3 versus -0.38Hz/s with OF1). Moreover, OF3 entails that APG controller of the HVDC links is set to ensure an optimal share of reserves among the areas. The optimal share of reserves of each area results in an effort to achieve similar dynamic frequency response in all areas. This implies that the supporting areas have less risk of stabilizing at a larger post disturbance steady state deviation compared to the affected area.

On the other hand, when the tuning is performed based on OF2, by using either the average speed or the COI for the calculations in (8) and (9), it can be observed in Figs. 15(b) and 15(c) that area C provides a more significant FFS compared to area B leading to worse frequency response in the former one compared to the latter one. The frequency performance of area C is affected by the APG of the HVDC link between A and C, which has a larger optimal ΔP (-300 MW) compared to the optimal ΔP (-100MW) calculated for the HVDC link between areas A and B, whereas no modulation occurs in the power flows of the HVDC link B to C. This is due to the fact that area C is electrically closer to the location of the active power imbalance. Note also in Figs. 11(b) and 11(c) that the affected area (area A) has a worse nadir (i.e. 49.64Hz), and steady state deviation (i.e. 49.80Hz) with respect to the case when OF1 and OF3 were used. Based on (11), the observations from Figs. 14(b) and 14(c) are attributed to the emphasis of OF2 on the minimization of derivatives of the relative frequencies between areas (cf. Fig. 10) during the transient period, leading to significantly different steady state frequency responses of the electrical areas according to the shared portion of the original imbalance. Moreover, in both versions of OF2, the RoCof encountered in the affected area is similar to the one obtained when OF1 is used. This shows that the considered time delay of 300ms in the activation of the HVDC links affects the degree of improvement of the RoCof in all problem formulations.

In terms of the method applicability, it is worth recalling from section III that OF1 and OF3 requires a trustworthy measurement of the area frequency, whereas OF2 requires the speeds of all the SGUs within each electrical area. The availability and trustworthiness of the measured area frequency or rotor speeds should be carefully taken into account in the application of these problem formulations in large systems with high-RES penetration or small number of SGUs.

Furthermore, Figs. 11(a) to 11(d) show that a local electromechanical oscillation is excited when FFS kicks-in. The active power imbalance occurring in area A disturbs the SGUs of this area, whose speed deviation and rotor angle state-variables have the highest participation factors in an oscillatory mode with frequency of approximately 1.4 Hz. Note in the figures that the damping factor (denoted as ζ) of the oscillation differs depending on the problem formulation used to coordinate FFS. Namely, ζ is in the order of 9%, 5%, and 7% when formulations 1, 2 or 3 are used, respectively. The significant difference of ζ between formulation 2 w.r.t. formulations 1 and 3 is due to the fact that formulation 2 attempts to coordinate FFS based on RoCoF, which exacerbates the acceleration of the SGUs. ζ of this oscillation mode can be improved by retuning the power system stabilizes attached to the SGUs. FFS control attached to electrolysers can also contribute to improve ζ in case it is implemented to emulate the behaviour of the SGUs. Such study will be addressed in a follow-up publication.

As far as the convergence rate is concerned, Figs. 12 and 13 show the convergence rate of OF1, OF2 and OF3 during the solution of the optimization problem. In Fig. 12 the optimization is based on a random initialization, whereas in Fig. 13 a predefined solution vector $\mathbf{x_0}$ is considered. The predefined initial solution vector corresponds to the pre disturbance power flow setpoints of the HVDC links. The convergence plots shown in Figs. 12 and 13 constitutes normalized data. The normalization is in the scale [0 100], where 100 is the value of each OF evaluated in the baseline case (when only SGU perform frequency control, cf. Fig. 10). Note in Figs. 12 and 13 that any of the OFs

requires less than 100 iterations to converge when the MVMO algorithm is used. This was empirically checked based on 1000 independent runs of the optimization. Random initialization was done in each run. For instance, the value of OF1 at 100 iterations or higher number of iterations was in the range [min=7.3434, max=7.9309], with mean=7.6371. By contrast, OF1 at 50 iterations was in the range [min=13.1281, max=14.7596], with mean=13.7478]. This highlights the limited sensitivity of MVMO (from 100 iterations for this optimization problem) to random factors involved in its evolutionary mechanism as well as its powerful adaptation between exploration and exploitation to significantly reduce OF within a relatively low computing budget. The number of iterations could be lower if the MVMO is optimally tuned. For sake of additional illustration, the appendix provides the outcomes of basic statistical performance evaluations done based on Wilcoxon rank sum, Friedman aligned, and Quade tests. This will be deeply addressed in a subsequent dedicated publication which will include additional statistical tests on the performance of MVMO as well as a comparative analysis with respect to other powerful optimization solvers from literature.

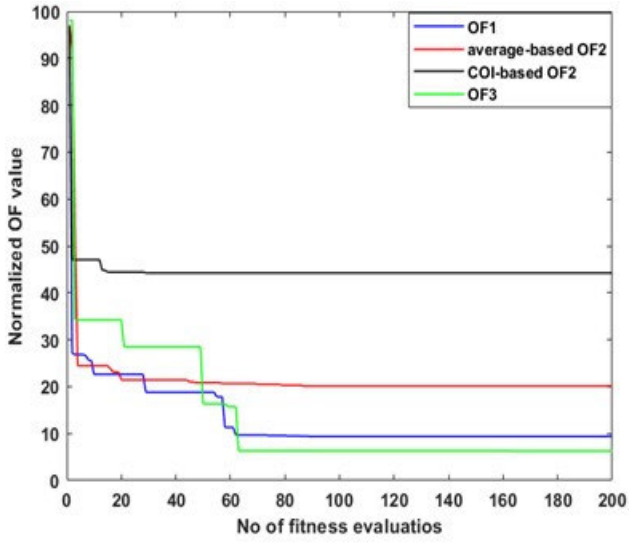

FIGURE 12. Convergence of OFs' value in Scenario 1 when a random x_0 is used.

Figs 12 and 13 also show that OF1 and OF3 can achieve a more significant minimization of their value compared to any variant of OF2. This attributed to the nature of OF2, which involves an attempt to minimize the derivatives of the relative frequency excursions during initial transient period after the occurrence of an active power imbalance, while also attempting to achieve a similar characteristic of the post-disturbance steady state frequency in each area.

By contrast, OF1 and OF3 attempt to minimize the point-to-point difference between the nominal frequency and the electrical areas' frequency and the difference between each pair of frequency responses, respectively. Also, note that the starting point of the optimization search can be compared

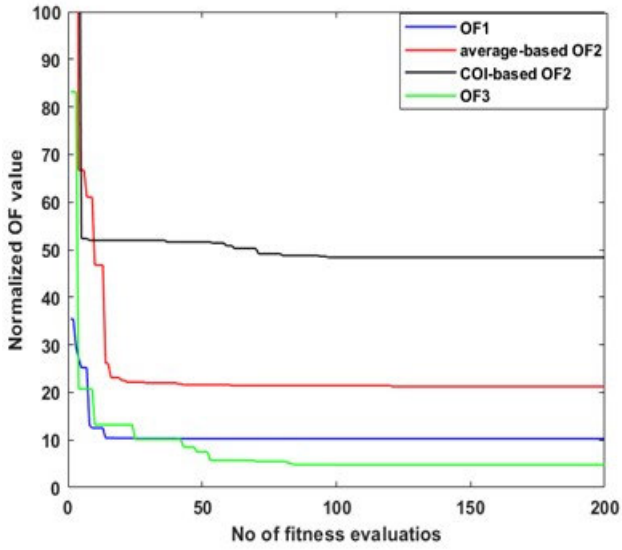

FIGURE 13. Convergence of OFs' value in Scenario 1 when a predefined x_0 is used.

when a predefined initial solution is used. Besides, it is inferred that the convergence of the OFs could be better if a better initial solution is used. This observation will be further examined in future studies focused on the randomness of the optimization search by MVMO.

B. SCENARIO 2

In this scenario, FFS is provided in area A not only through the modifications of the power flows of the HVDC links, but also from the PEM electrolyzers installed in each area. The share of FFS is distributed among the available PEI elements according to the tuned parameters of the APG controllers applied after solving the optimization problem. The tuning of the APG controllers is achieved by utilizing one of the proposed problem formulations. The frequency response obtained when problem formulations OF1, average-based OF2, COI-based OF2 and OF3 are used can be observed in Figs. 14(a) to 14(d), respectively.

In all examined cases, during the first second of the simulation, the frequency in all areas is constant at 50 Hz, experiencing a balanced pre-disturbance period. At t=1s, the SGU A1a (cf. Fig. 3) is set out of service, perturbing the active power balance in area A. The frequency in area A, deviates from its nominal value and the PEM electrolyzers installed in area A are activated to provide FFS. In the meantime, the frequency in areas B and C remains intact for 300ms following the disturbance, due to the activation time delay applied in the APG controllers of the HVDC links. After this period, the power flows of the HVDC links change according to the solution of the optimization problem utilizing one of the proposed problem formulations. In that way, the initial imbalance is shared to the other areas to be effectively contained. Hence, the active power imbalance in areas B and C is perturbed, and the frequency starts to drop. Then, in contrast to scenario 1,

the impact on the supporting areas is mitigated not only from the local SGUs, but also from the PEM electrolyzers installed in areas B and C. Consequently, electrolyzers are used to arrest the initial frequency drop in area A and to mitigate the impact on the supporting areas after the power flows on the HVDC links are modulated.

From Fig. 14, it can be seen that all frequency responses follow the same pattern with the ones obtained in scenario 1 (cf. Fig. 11). However, in all cases the support from the PEM electrolyzers leads to improved responses in terms of Nadir, RoCof and steady-state deviation. When OF1 is utilized(cf. Fig 14(a)), the frequency in the affected area has a Nadir of 49.72 Hz that subsequently stabilizes at 49.95 Hz and experiences a RoCoF of -0.33 Hz/s. This shows that the addition of the PEM electrolyzers can arrest the initial frequency drop and improve RoCof. Also, by comparing Figs 11(a) and 14(a), it is observed that the frequency in areas B and C deviates less from its nominal value. That is due to the fact that the electrolyzers are rapidly activated to minimize the impact on the supporting areas when the imbalance is shared to them through the HVDC links. Also, note from Fig. 14(a) that the continuous support from the electrolyzers minimizes the risk of larger steady state frequency deviations in the supporting areas compared to the affected area. That leads to an improved convergence of the frequency responses in Scenario 2 compared to Scenario 1. Consequently, the increase of the available PEI elements for FFS improves the frequency response in all areas in terms of Nadir, RoCoF and steady state deviation taking advantage of the response of these elements to sensed frequency deviations.

When OF3 is used to tune the APG controllers (cf. 14(d), the obtained frequency response is similar to the one obtained when tuning is performed by using OF1 (cf. 14(a)). The resulting frequency Nadir is equal to 49.72 Hz, experiencing a RoCoF of -0.33 Hz/s before stabilizing at 49.92 Hz. This shows that both OF1 and OF3 can lead to significantly improved responses compared to the baseline scenario and optimally share the imbalance among the available PEI elements that provide FFS. The obtained response tends to achieve a coupled dynamic frequency response for a decoupled system that has areas of different inertia and active power reserve characteristics.

On the other hand, when any of the OF2 variants are used, the obtained frequency responses for the affected area is worse compared to OF1 and OF3. That is due to the fact that OF2 aims to minimize the derivative of the relative frequency of each area focusing more on the transient period of the response rather than on its post-disturbance steady state deviation. However, when compared to Scenario 1, the addition of the electrolyzers leads to improved responses for all the interconnected areas. Area A experiences a nadir of 49.69 Hz that subsequently stabilizes at 49.84 Hz, whereas the initial RoCoF is equal to the one obtained when OF1 or OF3 is used. Also, the impact on the supporting areas is minimized although a similar pattern with Scenario 1 is

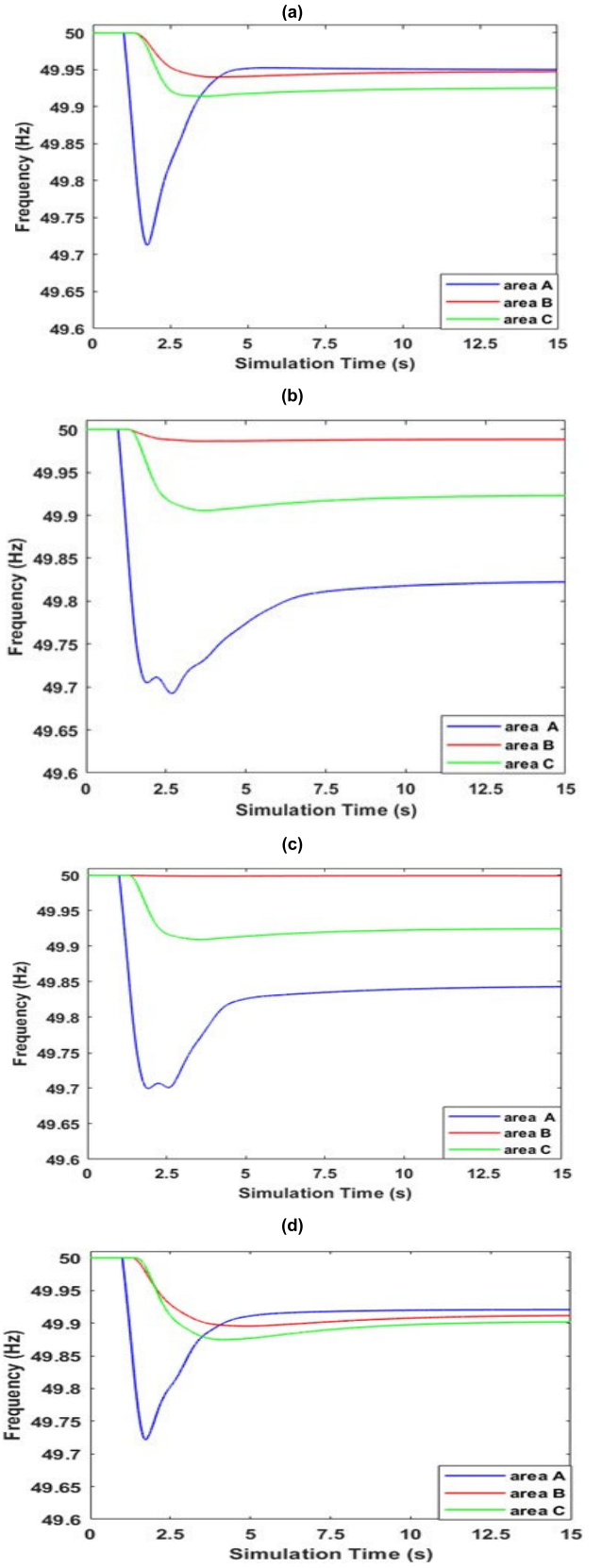

FIGURE 14. Frequency responses Scenario 2 – FFS by HVDC links and PEM electrolyzers a) tuning OF1 b) tuning average-based OF2 c) tuning COI-based OF2 d) tuning OF3.

followed. The latter refers to the fact that area C, the area that is electrically closer to the disturbance, is more significantly affected compared to area B. Consequently, it is evident that the addition of PEM electrolyzers can improve the obtained responses in terms of Nadir, RoCoF and steady state deviation due to the additionally provided active power, their rapid response to sensed frequency deviations, and the continuous support that they can offer. However, the utilization of OF2 for the tuning of the APG controllers leads to worse responses compared to OF1 and OF3.

Apart from the responses themselves, it is worth emphasizing that all the problem formulations can effectively tune the APG controllers even when the size of the optimization vector increases. However, in none of them the electrolyzers in the affected area are not tuned to offer their maximum support before the activation of the HVDC links. This shows that the optimization tends to share the imbalance among all the available sources of FFS rather than releasing first the local active power reserves in the affected area. That can be explained considering the fact that the HVDC links are characterized by a larger FFS capability in terms of magnitude and active power support rate over time compared to PEM electrolyzers. As far as the convergence rate is concerned, Figs. 15 and 16 show the convergence rate of OF1, OF2 and OF3 during the solution of the optimization problem. In Fig. 15 the optimization is based on a random initialization, whereas in Fig. 16 a predefined solution vector $\mathbf{x_0}$ is considered.

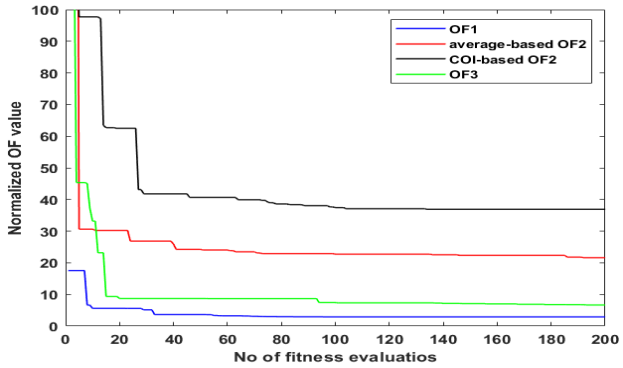

FIGURE 15. Convergence of OFs' value in Scenario 2 when a random x_0 is used.

The predefined initial solution vector corresponds with the pre disturbance power flow setpoints of the HVDC links and considering that the PEM electrolyzers is the affected area are tuned at their maximum support capability. This initial vector examines the case at which the local PEM electrolyzers are fully released before the activation of the HVDC links. The convergence plots shown in Figs. 15 and 16 constitute normalized data. The normalization is in the scale [0 100], where 100 is the value of each OF evaluated in the baseline case (when only SGU perform frequency control, cf. Fig. 11).

From Figs. 15 and 16 it is evident that any of the OFs require less 150 iterations to converge when the MVMO algorithm is used. However, the increase in the number of the

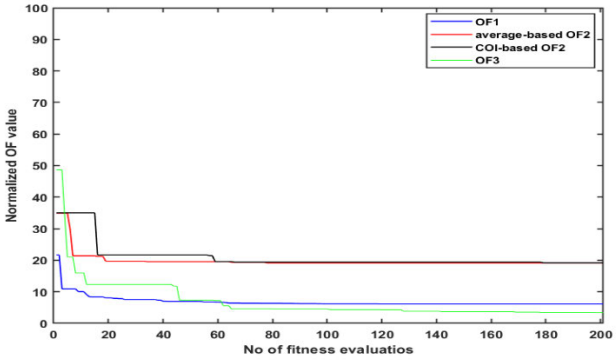

FIGURE 16. Convergence of OFs' value in Scenario 2 when a predefined x_0 is used.

optimization variables from 6 in Scenario 1 to 28 in Scenario 2 leads to an increased number of fitness evaluations required to converge. In any case, for a fourfold increase in the size of the optimization vector, a smaller than twofold increase in the number of fitness evaluations required is observed. This confirms the efficiency of the MVMO algorithm in solving complex problems. This number of iterations could be lower if the MVMO is optimally tuned. This will be addressed in a subsequent publication which will include statistical tests on the performance of MVMO as well as a comparative analysis with respect to other powerful optimization solvers from literature.

Moreover, similarly to Scenario 1, OF1 and OF3 can achieve a more significant minimization of their value compared to any variant of OF2. This is due to the complex nature of the OF2 as previously explained. Also, the addition of PEM electrolyzers for FFS, can lead to more significantly reduced OF values compared to Scenario 1. That is due to the fact that additional active power is available for frequency support for the affected area in the time frame of 300 ms before the activation of the HVDC links and the fast response of the electrolyzers in the supporting areas against the shared portion of the active power imbalance. The latter, leads to improved frequency responses in all areas and thus to a larger reduction of the OFs value. Finally, it is evident that the convergence of the OFs could be further improved if a suitable initial solution is used. This observation will be further examined in future studies focused on the randomness of the optimization search by MVMO.

VI. CONCLUSION

Maintaining frequency stability in power electronics–dominated systems is a key challenge for operators. Power electronic units such as WTs, PVs, ESSs, HVDC links, and PEM electrolyzers can provide FFS if properly controlled. Regulating active power and its ramp rate at converter outputs is a promising method to counter power–frequency imbalances, but coordinated tuning is essential when multiple units participate to prevent conflicting control actions.

This paper proposes three optimization problem formulations solved using the MVMO algorithm to coordinately tune APG controllers in MMC-based HVDC links and PEM electrolyzers within a multi-area hybrid HVDC-HVAC system under active power imbalances. Each formulation addresses frequency stability from a different angle: OF1 minimizes frequency deviations from the nominal value; OF2 minimizes and equalizes the rate of frequency change across areas; and OF3 minimizes differences between dynamic frequency responses, aiming to achieve coupled behavior in electromagnetically decoupled areas.

The optimization problem was solved through RMS simulations in a DIgSILENT PowerFactory 2024 SP2–Python 3.8 co-simulation setup. Frequency responses were compared against each other and a baseline without FFS to identify the best tuning strategy. Frequency performance was assessed by several metrics (Nadir, RoCoF, steady-state deviation), convergence rate, optimization efficiency, and applicability. Results showed OF2 performed worst across all scenarios: despite improving over the baseline, it failed to balance FFS contributions. By minimizing frequency derivatives, OF2 emphasized transients over steady-state performance, causing nearby areas to bear most of the imbalance and resulting in uneven dynamic responses.

OF1 and OF3 deliver much better frequency responses across all areas. OF1 prioritizes restoring the affected area to 50 Hz but can cause larger steady-state deviations in supporting areas. OF3 instead aims for coupled frequency behavior, improving Nadirs and RoCoFs but potentially worsening steady-state deviations as it equalizes area responses. Overall, adding PEM electrolyzers to frequency regulation mitigates these risks and yields similar responses for both OF1 and OF3. These responses are characterized by significantly improved nadir (from 48.8 Hz to 49.72 Hz), RoCoF (from -0.51 Hz/s to -0.33 Hz/s) and steady state deviation (from 49.55 Hz to 49.95 Hz) compared to the baseline scenario. Also, the frequency responses tend to have a similar post disturbance steady state behavior. Consequently, when OF1 and OF3 are used, an optimal share of FFS is achieved among the available reserves and the obtained frequency responses are significantly improved.

The response timing of system elements strongly influences frequency behavior across all formulations. HVDC links adjust power about 300 ms after a disturbance, limiting RoCoF improvement when electrolyzers are inactive. PEM electrolyzers help arresting the initial frequency deviation before HVDC action and reduce imbalance impacts on supporting areas afterward. Thus, increasing the number of well-coordinated FFS elements enhances frequency stability across all areas.

As far as the efficiency of the algorithm is concerned, it was proven that when the MVMO is used to solve the optimization problem, an optimal tuning can be achieved for the considered sizes of the optimization vector. When the size of $\mathbf{x}$ increases, a larger number of fitness evaluations is required for the OF value to converge. For instance, approximately 100 iterations are required when the formulations are analyzed under scenarios 1 (i.e., only HVDC links provide FFS), which entails 6 optimization variables. By contrast, 150-200 iterations are required in scenarios 2 (FFS provided by HVDC links and PEM electrolysers), which entails 28 optimization variables. The number of iterations may be significantly higher when the formulations are applied to large-size systems, which may involve optimization vectors with size in the order of dozens, hundreds, or thousands. This challenge can be tackled, for instance, by decomposing the formulations into smaller subproblems, solved in parallel, or by simplifying the formulations through dimensionality reduction supported by surrogate models. Acceleration techniques could also be explored, for instance, by considering graphic or quantum processing units. Providing a suitable initial vector $\mathbf{x_0}$ to the algorithm or tuning properly the MVMO may also significantly reduce the number of iterations required for convergence. However, this issue will be addressed in future research. OF1 and OF3 have been observed to achieve a more significantly reduced value of their OF value compared to the baseline case due to the better utilization of the FFS sources and compared to any variant of OF2. Finally, the addition of more controllable FFS elements lead to similar and improved OF values for OF1 and OF3 constituting them the most suitable problem formulations to tune the APG controllers.

Furthermore, future research studies will consider the adoption of the APG control strategy to other PEI elements such as WTs, PV systems, ESSs and EVs increasing the number of FFS elements with different dynamic responses. This could be also a challenge for coordinating them due to the increasing number of the optimization variables and the complexity of different responses encountered. A further improvement in the control loops of the APG control strategy and a definition of new problem formulations is a field that needs to be further investigated. Besides, it is worth pointing out that future works will individually tackle other stability phenomena like oscillatory stability (incl. multi-converter oscillations), voltage stability, converter driven stability, and resonance stability. As suggested in [4], each of these phenomena requires a specific (e,g. more detailed) modelling and analysis approach to properly study (i.e. understand and solve) the underlying peculiarities. Dedicated comprehensive future studies will individually address important subsequent research aspects motivated by this manuscript like controller robustness (e.g. considering noise, cyberattacks, latencies, measurement/communication failures), larger-size converter dominated systems (scalability of the optimization problem formulations), and multi-objective performance comparison against other solutions like artificial intelligence based methods or model predictive control.

APPENDIX

In this Section, the complete optimization vectors following the solution of the optimization problem utilizing the different problem formulations (i.e. OF1, OF2, and OF3) are compared to each other and to the pre disturbance values

of the corresponding optimization variables. In scenario 1, only HVDC links are activated for FFS, and thus, **x** contains 6 optimization variables, APG and ΔP, for the HVDC links AB, AC and BC respectively. Before the imbalance, the APG of all HVDC links is set to 0MW/s as no modifications are applied in their active power. The setpoint for active power are set to 600MW, 700MW and 100 MW flowing from areas A to B, A to C and C to B, respectively. Having solved the optimization problem using the MVMO, the optimization vector has the values shown in (16) to (18) with respect to the problem formulation utilized (i.e. OF1, OF2, OF3) respectively.

$$\mathbf{x}_{OF1} = \left[630\frac{MW}{s}, -80MW, 992\frac{MW}{s}, -561MW, 580\frac{MW}{s}, -308MW\right] \quad (16)$$

$$\mathbf{x}_{OF2} = \left[600\frac{MW}{s}, -88.43MW, 980\frac{MW}{s}, -316.6MW, 760.8\frac{MW}{s}, 0MW\right] \quad (17)$$

$$\mathbf{x}_{OF3} = \left[977\frac{MW}{s}, -270MW, 840\frac{MW}{s}, -271MW, 894\frac{MW}{s}, -58.17MW\right] \quad (18)$$

In this case it is clear that HVDC link AC, the one installed electrically closer to the disturbance, is the most significantly affected one considering its power flows in all cases. When OF1 is used, HVDC link A*B* reduces the power injection to area B from area A by 80MW, but at the same time HVDC link BC changes the direction of its power flow, so that area B will support area C as well. Hence, OF1 mitigates the impact on area A, the affected area, mainly by changing significantly the power flow in the HVDC link AC that is electrically closer to the imbalance and minimizes the impact on area C by regulating the power flows in HVDC link BC that interconnects the supporting areas. That is not the case when OF2 is considered. In this case, HVDC AC experiences the largest change in its active power flow, affecting significantly area C. However, HVDC link BC does not alter its active power setpoint and thus area C experiences a larger impact compared to area B.

Finally, in contrast to the other formulations OF3 tries to share the imbalance among the areas. Hence, an equal reduction of around 270MW is observed in HVDC links AB and AC interconnecting the affected area with the others. Also, HVDC link BC in this case reduces its power injection from area C to B to minimize the impact on the supporting area with the lowest inertia conditions. Consequently, it is clear that OF3 achieves an optimal share of the imbalance utilizing the HVDC links AB and AC equally and regulates the power exchange among the supporting areas to equalize the impact on them. The APG in all cases large amounts of active power is provided to the affected area is characterized by large ramp rates so that it can rapidly arrest the frequency deviations. That is an impact of the considered time delay applied in the activation of the HVDC links, that in this case requires a rapid response of the HVDC links. The convergence rate of the optimization variables in case OF3 is utilized, the formulation that achieved the best share of the imbalance in scenario 1 can be observed in Figs. 17 and 18 for the APG and P_{ref_new} (i.e $P_{ref\_new} = P_{ref} + \Delta P$) illustrated for comparison purposes in a normalized range [0,1] and [-1,1], respectively. These convergence plots (cf. Figs. 17 and 18), show that finding the optimal APG value for the HVDC links requires a larger number of iterations that to determine the ΔP in the HVDC links AB and AC. This shows that the rate a certain power injection is performed to the affected area is critical. On the other hand, in the HVDC link BC, a larger number of iterations is required to determine the setpoint of the link. That is due to the fact that this link has a supplementary role in sharing the imbalance among the supporting areas according to their inertia and active power reserve characteristics.

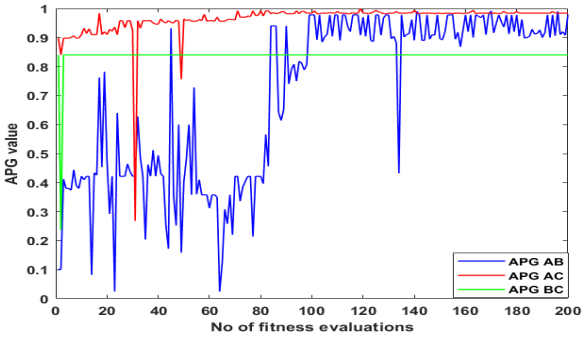

FIGURE 17. APG HVDC convergence using OF3 in scenario 1.

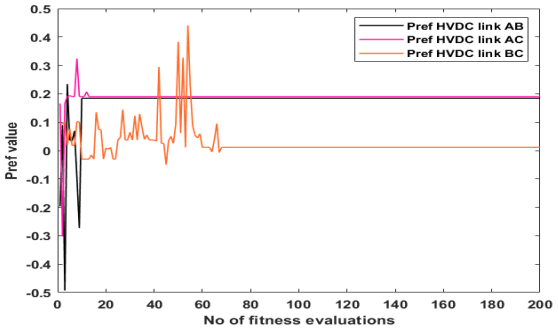

FIGURE 18. P_{ref_new} HVDC convergence using OF3 in scenario 1.

In scenario 2, FFS is provided not only from the HVDC links but also from PEM electrolyzers. This leads the size of the optimization vector at its full extend of 28 optimization variables. During pre-disturbance, the values of the corresponding optimization variables are equal to the solution of the power flow during steady state conditions and the APG of all units is equal to 0 as no changes in their active power outputs is applied. The obtained optimization vectors having solved the optimization problem with OF1, OF2 and OF3 can

be observed in (19) to (21) respectively.

$$\mathbf{x}_{OF1} = \Big[950\frac{MW}{s}, -474MW, 155\frac{MW}{s}, -130MW, 400\frac{MW}{s}, -200MW, 96.82MW, 13.88\frac{MW}{s}, 13MW, 46\frac{MW}{s}, 54MW, 73\frac{MW}{s}, 192MW, 153\frac{MW}{s}, 111MW, 86\frac{MW}{s}, 181.7MW, 118\frac{MW}{s}, 33MW, 29\frac{MW}{s}, 163MW, 118\frac{MW}{s}, 33MW, 24\frac{MW}{s}, 102MW, 147\frac{MW}{s}, 113MW, 68\frac{MW}{s}\Big] \quad (19)$$

$$\mathbf{x}_{OF2} = \Big[1000\frac{MW}{s}, 0MW, 1000\frac{MW}{s}, -278.17MW, 713\frac{MW}{s}, -48MW, 77MW, 68\frac{MW}{s}, 105MW, 45\frac{MW}{s}, 99MW, 75\frac{MW}{s}, 112MW, 43\frac{MW}{s}, 0MW, 0\frac{MW}{s}, 84MW, 100\frac{MW}{s}, 60MW, 48\frac{MW}{s}, 32MW, 0\frac{MW}{s}, 30MW, 0\frac{MW}{s}, 204MW, 92\frac{MW}{s}, 0MW, 50.6\frac{MW}{s}\Big] \quad (20)$$

$$\mathbf{x}_{OF3} = \Big[932\frac{MW}{s}, -185MW, 796\frac{MW}{s}, -377MW, 412\frac{MW}{s}, -189MW, 95.4MW, 67.5\frac{MW}{s}, 38.7MW, 72.2\frac{MW}{s}, 21.4MW, 62.3\frac{MW}{s}, 242MW, 121\frac{MW}{s}, 85.6MW, 29.2\frac{MW}{s}, 186MW, 36.7\frac{MW}{s}, 12.1MW, 16.4\frac{MW}{s}, 166MW, 74.5\frac{MW}{s}, 32.9MW, 24.7\frac{MW}{s}, 45.9MW, 94.5\frac{MW}{s}, 118MW, 53.5\frac{MW}{s}\Big] \quad (21)$$

In case OF1 is used, HVDC link AB is the one that experiences the most significant change in its power flow followed by HVDC link AC. That is due to the fact that area B is characterized by a large active power reserve from PEM electrolyzers and by a larger inertia. HVDC link BC similarly to scenario 1 tries to share the imbalance among the supporting areas. Considering the utilization of the PEM electrolyzers in this case, OF1 tends to use a 50% amount of their available reserve capacity in the affected area to arrest the initial frequency drop and then utilize a higher percentage of the available reserve from PEM electrolyzers installed in the supporting areas B and C to minimize the impact on them. Also, electrolyzers installed electrically closer either to the disturbance or to the CCPs of the HVDC links that share the imbalance to the supporting areas are more significantly affected. This confirms the significance of the location of installation of the active power reserves with respect to the imbalance.

In contrast, when OF2 is utilized, a higher share of the PEM electrolyzers in area A is released for FFS. Furthermore, only HVDC link AC, the one installed electrically closer to the imbalance, changes its power flow to sustain the frequency drop. PEM electrolyzers in other areas release a portion of the available reserve to minimize the impact on their active power balance sensed. Hence, OF2 tries to minimize the impact on the system frequency by using PEM electrolyzers and minimizing the change in the HVDC links power flows that may cause also large dP/dt in the other areas.

When OF3 is used the imbalance is shared to the supporting areas from HVDC links AB and AC. HVDC link BC then, balances the impact on the supporting areas with respect to the reserve characteristics of each area. PEM electrolyzers in area A are utilized to arrest the initial frequency drop before the activation of the HVDC links. Then the latter ones are used to inject active power to the affected area as they are able to provide a larger amount of active power at faster rates compared to the installed PEM electrolyzers in area A. Then PEM electrolyzers in areas B and C minimize the shared imbalance by reducing their active power consumption. Similarly to OF1, units installed electrically closer to the imbalance in area A or close to the CCPs of the HVDC links in the supporting areas are more significantly affected.

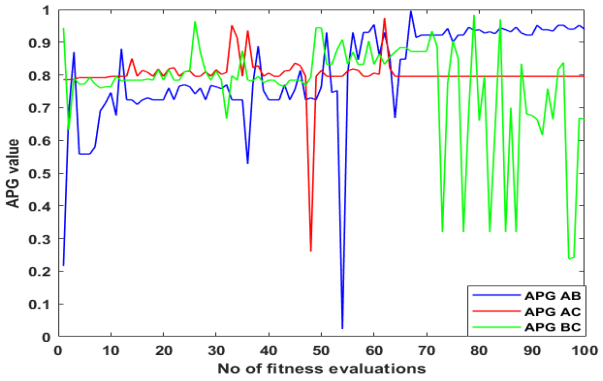

FIGURE 19. APG HVDC convergence using OF3 in scenario 2.

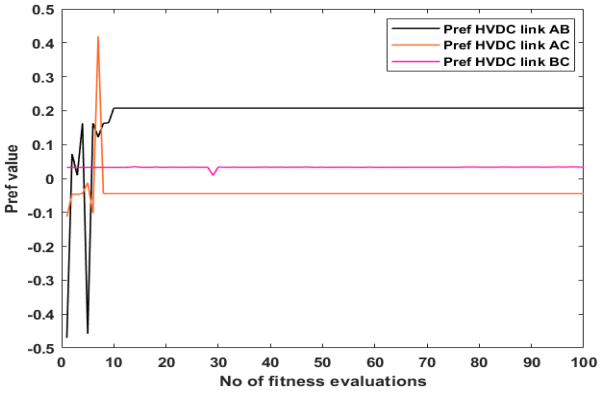

FIGURE 20. P_{ref_new} HVDC convergence using OF3 in scenario 2.

Figs. 19 to 22 show a typical convergence of the optimization variables for the HVDC links (cf. Figs. 19 and 20)

and PEM electrolyzers (cf. Figs. 21 and 22). For the APG variables and the active power consumption of the PEM electrolyzers the convergence values are in a normalized [0,1] range, whereas for the HVDC links active power setpoint in a [-1,1] range for illustration and comparison purposes. These plots show the significance of finding the optimal ramp rate in all units and the fact that a smaller number of iterations is required to determine the amount of the optimal power injection in the elements that have a larger accountability for FFS.

Table 3 summarizes computed performance metrics (i.e. mean, maximum, minimum) concerning with the objective function value (taking OF1 and scenario 2 as example) obtained by using MVMO and two optimization algorithms with proven performance in IEEE competitions on computationally challenging optimization problems [41]. The selected optimization algorithms are Differential Evolution with Success Rate-based adaptation (CL-SRDE) and Evolutionary Algorithm for COmplex-process oPtimization (EACOP). The recommended settings of MVMO, CL-SRDE, and EACOP were taken from [23], [42], and [43], respectively. A computing budget of maximum 100 function evaluations was considered in the application of each algorithm. Table 3 shows that MVMO is a competitive solver that can outperform the selected alternative solver. Table 3 also shows the results obtained by applying the Wilcoxon rank sum test, which was carried out by considering MVMO as the reference solver for pairwise comparison with the other two selected solvers. The outcomes of the test are represented by h values in Table 3, where h=1 entails that the solvers are statistically different with 95% certainty. The Friedman aligned rank test and the Quade test were also performed to additionally and empirically compare the performance of the three applied solvers. The results of are summarized in Table 4, highlighting that MVM statistically outperforms the other two selected solvers within the reduced computing budget and despite of the randomness of its evolutionary mechanism. The application and comparison of these solvers on lager dimensional versions of the presented optimization problem formulations will be presented in a subsequent publication.

TABLE 3. Performance of MVMO vs other solvers.

Metric\Solver	MVMO	CL-SRDE	EACOP
Maximum	7.9309	8.6358	9.8805
Mean	7.6371	8.2503	9.0361
Minimum	7.3434	8.0043	8.4449
H	1	1	1

For sake of supplementary illustration. the MVMO-based tuning is evaluated on an additionally modified version of the PST16 benchmark system, which includes a high-RES penetration scenario (i.e. 80% power supply from wind generation). Each wind power plan has wind generators equipped with direct-voltage type of grid forming control, multi-band power system stabilizers, and FFS in the form of virtual

TABLE 4. Ranking based on Friedman aligned and Quade tests.

Solver\Test	Friedman aligned	Quade
MVMO	7.4921	1.3547
CL-SRDE	8.5836	1.9862
EACOP	11.3284	2.4109

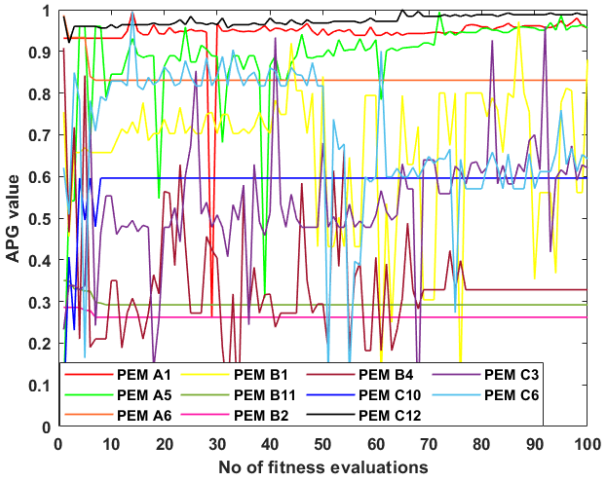

FIGURE 21. APG PEM electrolyzers convergence using OF3 in scenario 2.

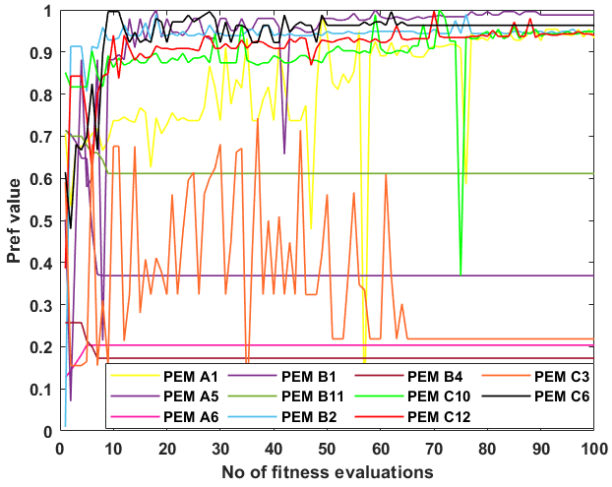

FIGURE 22. P_{ref_new} PEM electrolyzers convergence using OF3 in scenario 2.

synchronous power [45]. These controllers were tuned by parametric sensitivity before tackling the solution of the proposed formulation for FFS. Besides, the selected evaluated problem formulation OF1 was modified to include an inequality constraint imposing that any feasible solution must ensure that the worst damping oscillatory mode (of any frequency) must have a damping factor higher than 10%. The obtained frequency responses are shown in Fig. 23, illustrating a significantly improved dynamic performance, when all available power electronic converted interfaced devices, i.e. HVDC links, wind generation, and electrolyzers, are

optimally and coordinately tuned to deliver effective FFS, which quickly bounds the dynamic frequency deviation, also preventing exacerbated oscillations (collateral effect of effective arrest of active power imbalance combined with the included damping factor constraint in the optimization).

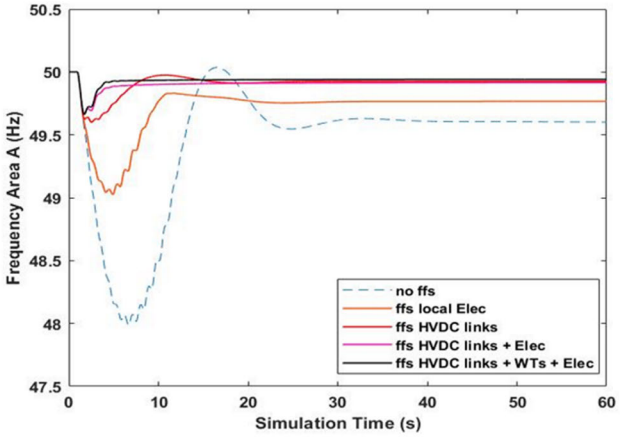

FIGURE 23. Frequency responses Scenario 1 – FFS by HVDC link, elecrolysers and wind power plants. Tuning considering OF1 with a damping factor constraint.

REFERENCES

[1] A. Halley, N. Martins, P. Gomes, D. Jacobson, W. Sattinger, Y. Fang, L. Haarla, Z. Emin, M. Val Escudero, S. Almeida De Graaff, V. Sewdien, and A. Bose, "Effects of increasing power electronics-based technology on power system stability: Performance and operations," *CIGRE Sci. Eng.*, vol. 11, pp. 5–17, Jun. 2018.

[2] A. Khan, M. Hosseinzadehtaher, M. B. Shadmand, S. Bayhan, and H. Abu-Rub, "On the stability of the power electronics-dominated grid: A new energy paradigm," *IEEE Ind. Electron. Mag.*, vol. 14, no. 4, pp. 65–78, Dec. 2020, doi: 10.1109/MIE.2020.3002523.

[3] X. Yuan, J. Hu, and S. Cheng, "Multi-time scale dynamics in power electronics-dominated power systems," *Frontiers Mech. Eng.*, vol. 12, no. 3, pp. 303–311, Sep. 2017, doi: 10.1007/s11465-017-0428-z.

[4] N. Hatziargyriou et al., "Definition and classification of power system stability—Revisited & extended," *IEEE Trans. Power Syst.*, vol. 36, no. 4, pp. 3271–3281, Jul. 2021, doi: 10.1109/TPWRS.2020.3041774.

[5] N. Hatziargyriou, J. V. Milanović, C. Rahmann, V. Ajjarapu, C. Cañizares, I. Erlich, D. Hill, I. Hiskens, I. Kamwa, B. Pal, P. Pourbeik, J. J. Sanchez-Gasca, A. Stanković, T. Van Cutsem, V. Vittal, and C. Vournas, "Definition and classification of power system stability–revised and extended," *IEEE Trans. Power Syst.*, vol. 38, no. 4, pp. 1787–1799, Dec. 2023.

[6] L. Meegahapola, A. Sguarezi, J. S. Bryant, M. Gu, E. R. Conde D., and R. B. A. Cunha, "Power system stability with power-electronic converter interfaced renewable power generation: Present issues and future trends," *Energies*, vol. 13, no. 13, p. 3441, Jul. 2020, doi: 10.3390/en13133441.

[7] V. N. Sewdien, R. Chatterjee, M. Val Escudero, and J. Van Putten, "System operational challenges from the energy transition," *CIGRE Sci. Eng.*, vol. 17, pp. 5–19, Feb. 2020.

[8] W. Wang, A. Beddard, M. Barnes, and O. Marjanovic, "Analysis of active power control for VSC–HVDC," *IEEE Trans. Power Del.*, vol. 29, no. 4, pp. 1978–1988, Aug. 2014.

[9] O. D. Adeuyi, M. Cheah-Mane, J. Liang, and N. Jenkins, "Fast frequency response from offshore multiterminal VSC–HVDC schemes," *IEEE Trans. Power Del.*, vol. 32, no. 6, pp. 2442–2452, Dec. 2017.

[10] M. Yu, A. Dysko, C. D. Booth, A. J. Roscoe, and J. Zhu, "A review of control methods for providing frequency response in VSC-HVDC transmission systems," in *Proc. 49th Int. Universities Power Eng. Conf. (UPEC)*, Sep. 2014, pp. 1–6.

[11] P. Maibach, A. Hernandez, J. Peiro, C. Smith, V. Sewdien, and J. van Putten, "Capabilities of power electronic devices in enabling the energy transition and mitigating system operational challenges," *CIGRE Sci. Eng.*, vol. 20, pp. 125–136, Feb. 2021.

[12] B.-I. Craciun, T. Kerekes, D. Sera, R. Teodorescu, and U. D. Annakkage, "Power ramp limitation capabilities of large PV power plants with active power reserves," *IEEE Trans. Sustain. Energy*, vol. 8, no. 2, pp. 573–581, Apr. 2017.

[13] A. Karaolanis, A. Perilla, J. L. Rueda, M. van der Meijden, and A. Alefragkis, "Generic model of a VSC-based HVDC link for RMS simulations in PSS/E," *IFAC-PapersOnLine*, vol. 51, no. 28, pp. 303–308, 2018.

[14] Á. Ortega and F. Milano, "Modeling, simulation, and comparison of control techniques for energy storage systems," *IEEE Trans. Power Syst.*, vol. 32, no. 3, pp. 2445–2454, May 2017, doi: 10.1109/TPWRS.2016.2602211.

[15] F. Alshehri, V. G. Suárez, J. L. Rueda Torres, A. Perilla, and M. A. M. M. van der Meijden, "Modelling and evaluation of PEM hydrogen technologies for frequency ancillary services in future multi-energy sustainable power systems," *Heliyon*, vol. 5, no. 4, pp. 1–24, Apr. 2019.

[16] A. D. Perilla Guerra, J. L. Rueda Torres, A. A. van der Meer, M. A. M. M. van der Meijden, and A. Alefragkis, "Influence of active power gradient control of an MMC-HVDC link on long-term frequency stability," in *Proc. IEEE Power Energy Soc. Gen. Meeting*, Chicago, IL, USA, Jul. 2017, pp. 1–5.

[17] E. Rakhshani, A. Perilla, J. L. R. Torres, F. M. Gonzalez-Longatt, T. B. Soeiro, and M. A. M. M. Van Der Meijden, "FAPI controller for frequency support in low-inertia power systems," *IEEE Open Access J. Power Energy*, vol. 7, pp. 276–286, 2020, doi: 10.1109/OAJPE.2020.3010224.

[18] E. Rakhshani, J. L. Rueda Torres, P. Palensky, and M. D. van Meijden, "Determination of maximum wind power penetration considering wind turbine fast frequency response," in *Proc. IEEE Milan PowerTech*, Jun. 2019, pp. 1–6, doi: 10.1109/PTC.2019.8810492.

[19] N. Veerakumar, Z. Ahmad, M. E. Adabi, J. L. Rueda Torres, P. Palensky, M. A. M. M. van der Meijden, and F. Gonzalez-Longatt, "Fast active power-frequency support methods in large scale electrolyzers for multi-energy systems," in *Proc. IEEE PES Innov. Smart Grid Technol. Eur. (ISGT-Europe)*, Oct. 2020, pp. 151–155.

[20] A. Perilla, D. Gusain, J. R. Torres, P. Palensky, M. van der Meijden, and F. Gonzalez-Longatt, "Optimal tuning of active power gradient control for frequency support in multi-energy systems," in *Proc. IEEE PES Innov. Smart Grid Technol. Eur. (ISGT-Europe)*, Oct. 2020, pp. 889–893.

[21] G. Giannakopoulos, A. Perilla, J. R. Torres, and P. Palensky, "A new formulation for optimal tuning of fast frequency support in multi-energy systems," in *Proc. IEEE Power Energy Soc. Gen. Meeting (PESGM)*, Denver, CO, USA, Jul. 2022, pp. 01–05.

[22] J. L. R. Torres, A. Perilla, E. Rakhshani, P. Palensky, M. A. A. M. van der Meijden, and A. Alefragkis, "MVMO-based tuning of active power gradient control of VSC-HVDC links for frequency support," in *Proc. 2nd Int. Conf. Smart Grid Renew. Energy (SGRE)*, Nov. 2019, pp. 1–6.

[23] J. L. Rueda and I. Erlich, "Hybrid single parent-offspring MVMO for solving CEC2018 computationally expensive problems," in *Proc. IEEE Congr. Evol. Comput. (CEC)*, Jul. 2018, pp. 1–8.

[24] S. P. Teeuwsen, "Oscillatory stability assessment of power systems using computational intelligence," Ph.D. dissertation, Univ. Duisburg-Essen, Duisburg, Germany, 2005.

[25] F. M. Gonzalez-Longatt and J. L. Rueda Torres, *PowerFactory Applications for Power System Analysis*. Cham, Switzerland: Springer, 2014.

[26] *Hydrogen Scaling Up—A Sustainable Pathway for the Global Energy Transition*, Hydrogen Council, Nov. 2017.

[27] *PowerFactory Seminar HVDC and Facts*, DIgSILENT GmbH, Gomaringen, Germany, Jun. 2018.

[28] *Guide for the Development of Models for HVDC Converters in a HVDC Grid*, CIGRE Working Group, Dec. 2014.

[29] N. Flourentzou, V. G. Agelidis, and G. D. Demetriades, "VSC-based HVDC power transmission systems: An overview," *IEEE Trans. Power Electron.*, vol. 24, no. 3, pp. 592–602, Mar. 2009.

[30] T. Shrivastava, A. M. Shandilya, and S. C. Gupta, "Overview strategy of wind farm in VSC-HVDC power transmission," in *Proc. IEEE 7th Power India Int. Conf. (PIICON)*, Bikaner, India, Nov. 2016, pp. 1–6.

[31] N.-T. Trinh, M. Zeller, K. Wuerflinger, and I. Erlich, "Generic model of MMC-VSC-HVDC for interaction study with AC power system," *IEEE Trans. Power Syst.*, vol. 31, no. 1, pp. 27–34, Jan. 2016.

[32] *Stability Analysis of an International Electricity System Connected to Regional Local Sustainable Gas Systems*, TSO, 2019.

[33] *FCR Manual for BSPs: Requirements and Procedures for Supply of FCR*, Tennet TSO, 2020.

[34] B. W. Tuinema, E. Adabi, P. K. S. Ayivor, V. García Suárez, L. Liu, A. Perilla, Z. Ahmad, J. L. Rueda Torres, M. A. M. M. van der Meijden, and P. Palensky, "Modelling of large-sized electrolysers for real-time simulation and study of the possibility of frequency support by electrolysers," *IET Gener., Transmiss. Distribution*, vol. 14, no. 10, pp. 1985–1992, May 2020.
[35] P. Kundur, *Power System Stability and Control*, 1st ed., New York, NY, USA: McGraw-Hill, 1994.
[36] W. Wang, A. Beddard, M. Barnes, and O. Marjanovic, "Analysis of active power control for VSC HVDC," *IEEE Trans. Power Del.*, vol. 29, no. 4, pp. 1978–1988, Aug. 2014.
[37] V. A. Martinez Lopez, H. Ziar, J. W. Haverkort, M. Zeman, and O. Isabella, "Dynamic operation of water electrolyzers: A review for applications in photovoltaic systems integration," *Renew. Sustain. Energy Rev.*, vol. 182, pp. 1–15, Aug. 2023.
[38] E. Rakhshani, D. Gusain, V. Sewdien, J. L. Rueda Torres, and M. A. M. M. Van Der Meijden, "A key performance indicator to assess the frequency stability of wind generation dominated power system," *IEEE Access*, vol. 7, pp. 130957–130969, 2019.
[39] *Commission Regulation (EU) 2017/1485 of 2 August 2017 Establishing a Guideline on Electricity Transmission System Operation*, Standard (EU) 2017/1485, European Commission, 2017.
[40] *Commission Regulation (EU) 2017/2196 of 24 November 2017 Establishing a Network Code on Electricity Emergency and Restoration*, Standard (EU) 2017/2196, European Commission, 2017.
[41] K. Qiao, X. Wen, X. Ban, P. Chen, K. V. Price, P. N. Suganthan, J. Liang, G. Wu, and C. Yue, "Evaluation criteria for CEC 2024 competition and special session on numerical optimization considering accuracy and speed," in *Proc. IEEE Congr. Evol. Comput. (CEC)*, Nov. 2023, pp. 1–12.
[42] V. Stanovov and E. Semenkin, "Differential evolution with success rate-based adaptation CL-SRDE for constrained optimization," in *Proc. IEEE Congr. Evol. Comput. (CEC)*, Jun. 2024, pp. 1–8.
[43] A. Tangherloni, V. Coelho, F. M. Buffa, and P. Cazzaniga, "A modified EACOP implementation for real-parameter single objective optimization problems," in *Proc. IEEE Congr. Evol. Comput. (CEC)*, Jun. 2024, pp. 1–8.
[44] B. E. Baningobera, I. Oleinikova, and K. Uhlen, "Optimizing frequency stability with adaptive fast frequency reserves and wide-area monitoring systems," *Int. J. Electr. Power Energy Syst.*, vol. 171, pp. 1–12, Oct. 2025.
[45] A. W. Korai, E. Rakhshani, M. E. Adabi, J. L. Rueda Torres, and M. A. M. M. van der Meijden, "Modelling and simulation of wind turbines with grid forming direct voltage control and black-start capability," in *Power Systems*, 2020, pp. 245–268.

GEORGIOS GIANNAKOPOULOS was born in Thessaloniki, Greece, in 1992. He received the M.Sc. degree in electrical power engineering from the Technical University of Delft, The Netherlands, in 2021. He is currently a Solar Battery Storage Specialist with Engineering and Construction Department, Enel Green Power, Hellas, where his work focuses on the design, integration, and optimization of utility-scale renewable energy projects, including solar, wind, and energy storage systems, with particular emphasis on their seamless integration into the electrical grid, also with Principa Energy, Athens, Greece, working as a Project Engineer with Solar and BESS Technologies. Prior to this role, he was a Research Assistant with the IEPG Group, TU Delft, investigating power system stability in grids with high renewable energy penetration. He also contributed to the design and implementation of microgrids in Sub-Saharan Africa with Gommyr Power Networks, advancing access to renewable energy in regions facing energy poverty and unreliable electrical infrastructure. His research interests encompass emerging renewable energy technologies, such as solar, wind, and energy storage systems, with a focus on their integration into the grid, and the development of smart grids and smart control strategies to enhance energy stability and reliability in modern power systems.

ARCADIO PERILLA received the B.S. degree in electrical power engineering from Universidad Simón Bolívar, Venezuela, in 2012, the M.Sc. degree from Université Lille 1–Sciences et Technologies, France, in 2015, and the Ph.D. degree in modern VSC-HVDC transmission systems from Delft University of Technology, The Netherlands, in 2023. He was a HVDC Technologist for the HVDC BiPole 2GW Program of the Transmission System Operator of the Netherlands, TenneT TSO. He is currently a Senior Simulation Engineer for multi-terminal BiPole VSC-HVDC transmission networks and renewable energy sources with ENOWA, Saudi Arabia, also with ABB, Madrid, Spain. He works as a Grid Integration Engineer. His research and professional interests include modeling and control of power electronics interfaced generation, dynamic stability assessment of power systems, and control of modular multilevel converters.

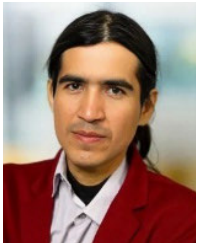

JOSÉ LUIS RUEDA TORRES (Senior Member, IEEE) was born in 1980. He received the Electrical Engineer Diploma degree (Hons.) from Escuela Politécnica Nacional, Quito, Ecuador, in August 2004, and the Ph.D. degree in electrical engineering from the National University of San Juan, obtaining the highest mark 'Sobresaliente' (Outstanding), in November 2009. From September 2003 to February 2005, he worked in Ecuador, in the fields of industrial control systems and electrical distribution networks operation and planning,. From August 2010 to February 2014, he was a Postdoctoral Research Associate with the Institute of Electrical Power Systems, University Duisburg-Essen, Duisburg, Germany. He is currently an Associate Professor leading the research team on dynamic stability of sustainable electrical power systems with the Intelligent Electrical Power Grids Section, Electrical Sustainable Energy Department, Delft University of Technology, Delft, The Netherlands. His research interests include physics-driven analysis of stability phenomena dynamic equivalencing of HVDC-HVAC systems, probabilistic multi-systemic reliability and stability management, and adaptive-optimal resilient multi-objective controller design. He is currently a member of the Technical Committee on Power and Energy Systems of IFAC (International Federation of Automatic Control), a Secretary of CIGRE JWG C4/C2.58/IEEE "Evaluation of Voltage Stability Assessment Methodologies in Transmission Systems", the Vice-Chair of the IEEE PES Intelligent Systems Subcommittee, and the Vice-Chair of the IFAC Technical Committee TC 6.3. Power and Energy Systems on social media.